High order finite difference methods with subcell resolution for advection equations with stiff source terms*

Wei Wang†, Chi-Wang Shu‡, H. C. Yee§, and Björn Sjögreen¶

August 23, 2011

Abstract

A new high order finite-difference method utilizing the idea of Harten ENO subcell resolution method is proposed for chemical reactive flows and combustion. In reaction problems, when the reaction time scale is very small, e.g., orders of magnitude smaller than the fluid dynamics time scales, the governing equations will become very stiff. Wrong propagation speed of discontinuity may occur due to the underresolved numerical solution in both space and time. The present proposed method is a modified fractional step method which solves the convection step and reaction step separately. In the convection step, any high order shock-capturing method can be used. In the reaction step, an ODE solver is applied but with the computed flow variables in the shock region modified by the Harten subcell resolution idea. For numerical experiments, a fifth-order finite-difference WENO scheme and its anti-diffusion WENO variant are considered. A wide range of 1D and 2D scalar and Euler system test cases are investigated. Studies indicate that for the considered test cases, the new method maintains high order accuracy in space for smooth flows, and for stiff source terms with discontinuities, it can capture the correct propagation speed of discontinuities in very coarse meshes with reasonable CFL numbers.

Key words: stiff reaction term, shock capturing, detonation, WENO, ENO subcell resolution

*This paper is an expanded version of "High-order finite difference methods with subcell resolution for hyperbolic conservation laws with stiff reaction terms: preliminary results" in Stanford CTR Annual Research Briefs 2010.

†Department of Mathematics and Statistics, Florida International University, Miami, FL 33199

‡Division of Applied Mathematics, Brown University, Providence, RI 02912

§NASA Ames Research Center, Moffett Field, CA 94035

¶Lawrence Livermore National Laboratory, Livermore, CA 94551

1 Introduction

In simulating hyperbolic conservation laws in conjunction with an inhomogeneous stiff source term, if the solution is discontinuous, spurious numerical results may be produced due to different time scales of the transport part and the source term. This numerical issue often arises in combustion and high speed chemical reacting flows.

The reactive Euler equations in two dimensions have the form

$$U_t + F(U)_x + G(U)_y = S(U), \tag{1}$$

where U, $F(U)$, $G(U)$ and $S(U)$ are vectors. If the time scale of the ordinary differential equation (ODE) $U_t = S(U)$ for the source term is orders of magnitude smaller than the time scale of the homogeneous conservation law $U_t + F(U)_x + G(U)_y = 0$ then the problem is said to be stiff. In high speed chemical reacting flows, the source term represents the chemical reactions which may be much faster than the gas flow. This leads to problems of numerical stiffness. Insufficient spatial/temporal resolution may cause an incorrect propagation speed of discontinuities and nonphysical states for standard dissipative numerical methods.

This numerical phenomenon was first observed by Colella et al. [13] in 1986 who considered both the reactive Euler equations and a simplified system obtained by coupling the inviscid Burgers equation with a single convection/reaction equation. LeVeque and Yee [23] showed that a similar spurious propagation phenomenon can be observed even with scalar equations, by properly defining a model problem with a stiff source term. They introduced and studied the simple one-dimensional scalar conservation law with an added nonhomogeneous parameter dependent source term

$$u_t + u_x = S(u), \tag{2}$$

$$S(u) = -\mu u(u - \frac{1}{2})(u - 1), \tag{3}$$

where the parameter $\frac{1}{\mu}$ can be described as the reaction time. When μ is very large, a wrong shock speed phenomenon will be observed in a coarse mesh. In order to isolate the problem, LeVeque and Yee solve (2) and (3) by the fractional step method. For the particular source term, the reaction (ODE) step of the fractional step method can be solved exactly. They found that the propagation error is due to the numerical dissipation contained in the scheme, which smears the discontinuity front and activates the source term in a nonphysical manner. By increasing the spatial resolution by an order of magnitude, they were able to improve towards the correct propagation speed.

It is noted that, in a general stiff source term problem, a sufficient spatial resolution is as important as temporal resolution when the reaction step of the fractional step method cannot be solved exactly. A study linking spurious numerical standing waves

for (2) and (3) by first and second-order spatial and temporal discretizations can be found in Lafon and Yee [22, 21] and Griffiths, Stuart and Yee [15].

For the last two decades, this spurious numerics phenomenon has attracted a large volume of research work in the literature (see, e.g., [5, 28, 6, 32, 8, 15, 24, 1, 7, 27]). Various strategies have been proposed to overcome this difficulty. Since numerical dissipation that spreads the discontinuity front is the cause of the wrong propagation speed of discontinuities, a natural strategy is to avoid any numerical dissipation in the scheme. In combustion, level set and front tracking methods were used to track the wave front to minimize this spurious behavior [24, 1, 7, 27]. In [11, 12], Chorin introduced the random choice method which is based on the exact solution of Riemann problems at randomly chosen locations within the computational cells and does not need to introduce any viscosity. It has been successfully used in [13, 25] for the solution of underresolved detonation waves. However, it is difficult to eliminate all numerical viscosity in a shock-capturing scheme. There are also many works on modifying shock-capturing methods for this problem in the literature. Fractional step methods are commonly used for allowing an underresolved meshsize. Such methods solve the homogeneous conservation law (i.e., the convection step) and the ODE system (i.e., the reaction step) separately. In [9, 10], Chang applied Harten's subcell resolution method [16] in a finite volume ENO method in the convection step with exact time evolution, which is able to produce a zero viscosity shock profile in the nonreacting flow. The time evolution is advanced along the characteristic line. Correct results were shown in the one-dimensional scalar case. However it seems difficult to extend this method to one-dimensional systems or multi-dimensional scalar equations or systems, due to the requirement of exact time evolution. In [14], Engquist and Sjögreen proposed a simple temperature extrapolation method based on a finite difference ENO scheme with implicit Runge-Kutta time discretization, which uses a first/second order extrapolation of the temperature value from outside the shock profile. Their approach is easily extended to multi-dimensions. However, their method is not a fractional step method, and it does not work well in the situation of insufficient spatial resolution. Hezel et al. [17] presented a modified fractional step method for detonation waves in which the exact Riemann solution is used to determine where burning should occur. Bao and Jin [2, 3, 4] proposed a random projection method based on the fractional step method where in the convection step a standard shock-capturing scheme is used, and in the reaction step a projection is performed to make the ignition temperature random. They have successfully applied this method to various problems in one- and two-dimensions. However they assume an *a priori* stiff source. In [33], Tosatto and Vigevano proposed a MinMax scheme, which is based on a two-value variable reconstruction within each cell, where the appropriate maximum and minimum values of the unknown are considered. The scheme may be applied with no difficulties to both stiff and nonstiff problems. Only one-dimensional problems were tested. However, it seems difficult to generalize either the random projection method or

the MinMax method to higher order accuracy. There are other works in the literature for stiff source hydrodynamics, e.g. [26].

Our objective in this study is to develop a high order finite difference method which can capture the correct detonation speed in an underresolved mesh and will maintain high order accuracy in the smooth part of the flow. The first step of the proposed fractional step method is the convection step which solves the homogeneous hyperbolic conservation law in which any high-resolution shock-capturing method can be used. The aim in this step is to produce a sharp wave front, but some numerical dissipation is allowed. The second step is the reaction step where an ODE solver is applied with modified transition points. Here, by transition points, we refer to the smeared numerical solution in the shock region, which is due to the dissipativity of a shock-capturing scheme. Because the transition points in the convection step will result in large erroneous values of the source term if the source term is stiff, we first identify these points and then extrapolate them by a reconstructed polynomial using the idea of Harten's subcell resolution method. Unlike Chang's approach, we apply Harten's subcell resolution in the reaction step. Thus our approach is flexible in allowing any shock-capturing scheme as the convection operator. In the reaction step, since the extrapolation is based on the high order reconstruction, high order accuracy can be achieved in space. The only drawback in our current approach is that the temporal accuracy will only be, at most, second-order due to the time splitting, which is common for most of the previous methods for stiff sources. We also remark that, in order to resolve the sharp reaction zone, sufficiently many grid points in this zone are still needed. The proposed method can capture the correct location and jump size of the reaction front, but it does not resolve the narrow reaction zone as typically there is one or less point in that zone.

This paper is organized as follows. Section 2 introduces the proposed fractional step method with subcell resolution for the one-dimensional scalar model problem in [23]. The high order accuracy of the method and its capability of capturing the correct speed of propagation of discontinuity are illustrated with numerical examples. The proposed method is extended to two-dimensional scalar problems with numerical examples in Section 3. In Section 4 the method is extended to one-dimensional reactive Euler equations with a one-step reaction. The numerical examples include the Chapman-Jouguet (C-J) detonation waves. The method is extended to two-dimensional reactive Euler equations in Section 5 and demonstrated by one numerical example. Section 6 contains the conclusion and remarks on future work.

2 Numerical method for 1D scalar problems

We first introduce the proposed method for the scalar model problem in [23], i.e.,

$$u_t + f(u)_x = S(u), \tag{4}$$

$$S(u) = -\mu u\,(u-\alpha)\,(u-1), \tag{5}$$

with the initial condition

$$u(x,0) = \begin{cases} 1, & x \le x_0 \\ 0, & x > x_0 \end{cases}, \tag{6}$$

where α is a parameter, $0 < \alpha < 1$, and x_0 is the position of the initial discontinuity.

The general fractional step approach is as follows. The numerical solution at time level t_{n+1} is approximated by

$$u^{n+1} = R(\Delta t)A(\Delta t)u^n. \tag{7}$$

The convection operator A is defined to approximate the solution of the homogeneous part of the problem on the time interval, i.e.,

$$u_t + f(u)_x = 0, \quad t_n \le t \le t_{n+1}. \tag{8}$$

The reaction operator R is defined to approximate the solution on a time step of the reaction problem:

$$\frac{du}{dt} = S(u), \quad t_n \le t \le t_{n+1}. \tag{9}$$

In the Strang-splitting in [31], the numerical solution at time step t_{n+1} is computed by

$$u^{n+1} = A\left(\frac{\Delta t}{2}\right) R(\Delta t) A\left(\frac{\Delta t}{2}\right) u^n, \tag{10}$$

where the convection operator is over a time step Δt and the reaction operator is over $\Delta t/2$. The two half-step reaction operations over adjacent time steps can be combined to save cost. The Strang-splitting (10) is used in this paper.

Next, we introduce the proposed fractional step methods for the convection step and the reaction step separately.

2.1 Convection operator

Any high resolution shock capturing operator can be used in the convection step. The purpose in this step is to minimize the transition points in the shock region. In this paper, we use the framework of high order finite difference WENO schemes [19] with a TVD Runge-Kutta time discretization to solve the one-dimensional scalar conservation law

$$u_t + f(u)_x = 0. \tag{11}$$

In particular, for the scalar case, we are interested in applying the anti-diffusive flux corrections [34] for the WENO scheme to obtain sharp resolution for contact discontinuities. In this section, we will briefly introduce this anti-diffusive WENO scheme for Eq. (11).

Let x_i, $i = 1, \ldots, N$ be a uniform (for simplicity) mesh of the computational domain, with mesh size $\Delta x = x_{i+1} - x_i$. An explicit conservative fully discrete finite difference scheme has the form

$$u_i^{n+1} - u_i^n + \lambda(\hat{f}_{i+1/2}^n - \hat{f}_{i-1/2}^n) = 0, \tag{12}$$

where u_i^n is the approximation to the point value $u(x_i, t_n)$, $\lambda = \Delta t/\Delta x$, and $\hat{f}_{i+1/2}^n$ is the numerical flux.

2.1.1 Modified TVD Runge-Kutta time discretization for anti-diffusive WENO schemes

The third-order TVD Runge-Kutta (RK3) time discretization [29] can be written as

$$\begin{aligned} u^{(1)} &= u^n + \Delta t L(u^n), & (13)\\ u^{(2)} &= u^n + \frac{1}{4}\Delta t L(u^n) + \frac{1}{4}\Delta t L(u^{(1)}), & (14)\\ u^{n+1} &= u^n + \frac{1}{6}\Delta t L(u^n) + \frac{1}{6}\Delta t L(u^{(1)}) + \frac{2}{3}\Delta t L(u^{(2)}), & (15) \end{aligned}$$

where L is the spatial discretization of $-f(u)_x$. The modified Runge-Kutta time discretization for anti-diffusive WENO schemes [34] is given by

$$\begin{aligned} u^{(1)} &= u^n + \Delta t L^{(1)}(u^n), & (16)\\ u^{(2)} &= u^n + \frac{1}{4}\Delta t L^{(2)}(u^n) + \frac{1}{4}\Delta t L^{(1)}(u^{(1)}), & (17)\\ u^{n+1} &= u^n + \frac{1}{6}\Delta t L^{(3)}(u^n) + \frac{1}{6}\Delta t L^{(1)}(u^{(1)}) + \frac{2}{3}\Delta t L^{(1)}(u^{(2)}), & (18) \end{aligned}$$

where the operators $L^{(k)}$ are defined as

$$L^{(k)}(u)_i = -(\hat{f}_{i+1/2}^{(k)} - \hat{f}_{i-1/2}^{(k)})/\Delta x, \quad k = 1, 2, 3, \tag{19}$$

with the anti-diffusive flux $\hat{f}_{i+1/2}^{(1)}$ and the modified anti-diffusive fluxes $\hat{f}_{i+1/2}^{(2)}$ and $\hat{f}_{i+1/2}^{(3)}$ defined in the next subsection.

2.1.2 Anti-diffusive flux with high order WENO finite difference reconstruction

The anti-diffusive flux for WENO scheme with RK3 is defined by

$$\hat{f}_{i+1/2}^{(1)} = \hat{f}_{i+1/2}^{-} + \phi_i \text{minmod}\left(\frac{u_i - u_{i-1}}{\lambda} + \hat{f}_{i-1/2}^{-} - \hat{f}_{i+1/2}^{-}, \hat{f}_{i+1/2}^{+} - \hat{f}_{i+1/2}^{-}\right), \tag{20}$$

where

$$\text{minmod}(a,b) = \text{sgn}(a)\cdot\max\{0,\min[|a|, b\,\text{sgn}(a)]\}, \tag{21}$$

$\hat{f}^-_{i+1/2}$ and $\hat{f}^+_{i+1/2}$ are the two upwind biased fluxes based on WENO stencils with one more point to the left and to the right, respectively. For WENO-Roe schemes, the numerical flux is chosen as $\hat{f}^-_{i+1/2}$ for $f'(u) > 0$ and $\hat{f}^+_{i+1/2}$ for $f'(u) < 0$.

The function ϕ is a discontinuity indicator which is close to 0 in smooth regions and close to 1 near a discontinuity. The indicator ϕ in [34] is

$$\phi_i = \frac{\beta_i}{\beta_i + \gamma_i}, \tag{22}$$

where

$$\alpha_i = |u_{i-1} - u_i|^2 + \varepsilon, \quad \beta_i = \left(\frac{\alpha_i}{\alpha_{i-1}} + \frac{\alpha_{i+1}}{\alpha_{i+2}}\right)^2, \quad \gamma_i = \frac{|u_{\max} - u_{\min}|^2}{\alpha_i}, \tag{23}$$

where ε is a small positive number (taken as 10^{-6} in the numerical experiments), and $u_{\max}$ and $u_{\min}$ are the maximum and minimum values of u_j over all grid points. We can see $0 \le \phi \le 1$, and $\phi_i = O(\Delta x^2)$ in smooth regions and ϕ is close to 1 near a discontinuity.

$\hat{f}^{(2)}_{i+1/2}$ and $\hat{f}^{(3)}_{i+1/2}$ are modifications of fluxes to the anti-diffusive flux $\hat{f}^{(1)}_{i+1/2}$.

$$\hat{f}^{(2)}_{i+1/2} = \begin{cases} \hat{f}_{i+1/2} + \text{minmod}\left(\frac{4(u_i - u_{i-1})}{\lambda} + \hat{f}^-_{i-1/2} - \hat{f}^-_{i+1/2}, \hat{f}^+_{i+1/2} - \hat{f}^-_{i+1/2}\right), & bc > 0, \quad |b| < |c|, \\ \hat{f}^{(1)}_{i+1/2}, & \text{otherwise}, \end{cases} \tag{24}$$

and

$$\hat{f}^{(3)}_{i+1/2} = \begin{cases} \hat{f}_{i+1/2} + \text{minmod}\left(\frac{6(u_i - u_{i-1})}{\lambda} + \hat{f}^-_{i-1/2} - \hat{f}^-_{i+1/2}, \hat{f}^+_{i+1/2} - \hat{f}^-_{i+1/2}\right), & bc > 0, \quad |b| < |c|, \\ \hat{f}^{(1)}_{i+1/2}, & \text{otherwise}, \end{cases} \tag{25}$$

where $b = \frac{u_i - u_{i-1}}{\lambda} + \hat{f}^-_{i-1/2} - \hat{f}^-_{i+1/2}$, and $c = \hat{f}^+_{i+1/2} - \hat{f}^-_{i+1/2}$.

The idea of constructing the anti-diffusive fluxes is to maintain a numerical traveling wave solutions for a piecewise constant function in order to avoid progressively smeared discontinuity front with time. The purpose of the extra factors 1, 4 and 6 in the first argument of the minmod function in the definition of $\hat{f}^{(k)}_{i+1/2}$ $(k = 1, 2, 3)$ is to compensate for the coefficients 1, $\frac{1}{4}$ and $\frac{1}{6}$ in front of $L^{(k)}$ $(k = 1, 2, 3)$, respectively. It has been numerically proved that, for a linear problem (i.e., $u_t + au_x = 0$) with a piecewise constant initial condition with two values, the linear scheme (i.e., $\hat{f}_{i+1/2} = f(u_i)$ for $a > 0$) will not have more than two transition points between two constant pieces for the CFL condition $a\lambda = a\Delta t/\Delta x \le \frac{1}{2}$ regardless of how long one runs the simulation.

We refer to [34] for more details about anti-diffusive WENO scheme in two dimensions and will not repeat them here.

2.2 Reaction operator

If there is no smearing of discontinuities in the convection step, any ODE solver can be used as the reaction operator. However, all the standard shock-capturing schemes will produce a few transition points in the shock when solving the convection equation. These transition points are usually responsible for causing incorrect numerical results in the stiff case. Thus we cannot directly apply a standard ODE solver at these transition points.

Here we use Harten's subcell resolution technique in the reaction step. The general idea is as follows. If a point is considered a transition point of the shock, information from its neighboring points which are deemed not transition points will be used instead.

The procedure can be summarized in the following steps:

(1) Use a "shock indicator" to identify cells in which discontinuities are believed to be situated. We consider the following minmod-based shock indicator in [16, 30]. Let

$$s_i = \text{minmod}\{u_{i+1} - u_i, u_i - u_{i-1}\}, \tag{26}$$

define the cell I_i as troubled if $|s_i| \geq |s_{i-1}|$ and $|s_i| \geq |s_{i+1}|$, with at least one being a strict inequality. Notice that this troubled cell-identifying method will only find the "worst" cell inside a shock transition. That is, if there are several consecutive transition cells, only the worst one will be identified as a troubled cell.

(2) In a troubled cell identified above, we continue to identify its neighboring cells. For example, we can define I_{i+1} as troubled if $|s_{i+1}| \geq |s_{i-1}|$ and $|s_{i+1}| \geq |s_{i+2}|$ and similarly define I_{i-1} as troubled if $|s_{i-1}| \geq |s_{i-2}|$ and $|s_{i-1}| \geq |s_{i+1}|$. If the cell I_{i-s} and the cell I_{i+r} $(s, r > 0)$ are the first good cells from the left and the right (i.e., I_{i-s+1} and I_{i+r-1} are still troubled cells), we compute the fifth order ENO interpolation polynomial $p_{i-s}(x)$ and $p_{i+r}(x)$ for the cells I_{i-s} and I_{i+r}, respectively. Because of the anti-diffusive corrector in the convection step, r and s will not be larger than 2 in general. The modified cell point value u_i is computed by

$$\tilde{u}_i = \begin{cases} p_{i-s}(x_i), & \theta \geq x_i \\ p_{i+r}(x_i), & \theta < x_i \end{cases}, \tag{27}$$

where the location θ is determined by conservation

$$\int_{x_{i-1/2}}^{\theta} p_{i-s}(x)dx + \int_{\theta}^{x_{i+1/2}} p_{i+r}(x)dx = u_i \, \Delta x. \tag{28}$$

Under certain conditions, it can be shown that there is a unique θ satisfying Eq. (28), which can be solved using, for example, a Newton's method. If there is no solution for θ or there are more than one solution, we choose $\tilde{u}_i = u_{i+r}$. Actually there is no difference to take $\tilde{u}_i$ from left or right for the scalar case because the source term will

be zero when $u_i = 0$ or 1. However, in the system case we would like to have the shock travel ahead of the reaction zone, so we take the value of u ahead of the shock.

(3) Use $\tilde{u}_i$ instead of u_i in the ODE solver if the cell I_i is a troubled cell.

For simplicity, consider the Euler forward method

$$u_i^{n+1} = u_i^n + \Delta t S(u_i^n), \tag{29}$$

Eq. (29) is modified to

$$u_i^{n+1} = u_i^n + \Delta t S(\tilde{u}_i), \tag{30}$$

if the cell I_i is a troubled cell.

Here we would like to remark that, implicit methods cannot be used in this step because the troubled values u_i^n need to be modified explicitly. However, there is no small time step restriction in the explicit method used here, because once the stiff points have been modified, the modified source term $S(\tilde{u}_j)$ is no longer stiff. Therefore, a regular CFL number is allowed in the explicit method.

For the scalar case, the second-order linearized trapezoidal method is used in the numerical examples

$$u_i^{n+1} = u_i^n + \frac{\Delta t S(u_i^n)}{1 - \frac{\Delta t}{2} S'(u_i^n)}. \tag{31}$$

Remark 2.1. *In general, the anti-diffusive WENO scheme can capture the discontinuity sharply with, at most, two transition points inside the discontinuity. Thus it does help for the stiff source term problems. For example, in the numerical computation, we use the two immediate neighboring cells ($s = r = 1$) for the subcell resolution procedure. This works because the anti-diffusive WENO scheme provides a very sharp shock front in the convection step. However, if the standard WENO scheme is used instead, more neighboring cells need to be identified ($s, r > 1$) for the subcell resolution procedure.*

Remark 2.2. *If a multi-step ODE solver is applied in the reaction step, a modification of the transition points in each step is required.*

Remark 2.3. *The proposed method is valid for a general $f(u)$ and a general $S(u)$.*

2.3 Numerical examples of 1D scalar problems

In this section, we test the proposed method on three scalar problems. The proposed method uses a fifth-order WENO-Roe scheme (WENO5) with the third-order TVD Runge-Kutta method (RK3) as the convection operator, and a linearized trapezoidal method (31) based on the subcell resolution (SR) as the reaction operator. From now on, we use the notation WENO5/SR for the proposed WENO scheme. If the fifth-order anti-diffusive WENO is used in the convection step, the notation anti-diffusive WENO5/SR will be used.

Table 1: L_1 errors and orders of accuracy by the anti-diffusive WENO5/SR at $t = 0.3$ with CFL=0.6.

N	error	order
10	1.02E-02	–
20	4.06E-04	4.65
40	1.21E-05	5.07
80	3.71E-07	5.03
160	1.18E-08	4.98

Example 2.1. Accuracy test.

We first test the convergence order of the proposed anti-diffusive WENO5/SR scheme. We consider Eq. (4) with $f(u) = u$ and the source term

$$S(u) = -u + \sin(2\pi(x - t)) \tag{32}$$

and periodic boundary conditions on the computation domain $x \in [0, 1]$. The exact solution is $u(x, t) = \sin(2\pi(x-t))$. The errors and orders of accuracy are listed in Table 1. Since both the Strang splitting method and also the trapezoidal rule in the reaction step are second-order in time, we set $\Delta t = \text{CFL} \times (\Delta x)^{5/2}$ to achieve the fifth order in space as shown in Table 1.

The next examples are to show the ability of the proposed schemes to deal with the propagating shocks.

Example 2.2. 1D scalar test case of a linear $f(u)$.

This example is the model problem of [23]. Consider Eq. (4) with $f(u) = u$, the source term given by Eq. (5) with $\alpha = 0.5$, and the initial condition:

$$u(x, 0) = \begin{cases} 1, & x \le 0.3 \\ 0, & x > 0.3 \end{cases}. \tag{33}$$

For this initial value problem, the exact solution is

$$u(x, t) = \begin{cases} 1, & x \le t + 0.3 \\ 0, & x > t + 0.3 \end{cases}. \tag{34}$$

Analytically, the source term should be always zero. However, if μ in the source term Eq. (5) is very large, the numerical errors of u in the transition region can result in large erroneous values of $S(u)$, which must be corrected.

We compare the numerical results by the anti-diffusive WENO5/SR and the WENO5 with splitting (denoted by splitting WENO5) in Figs. 1 and 2, respectively. For each

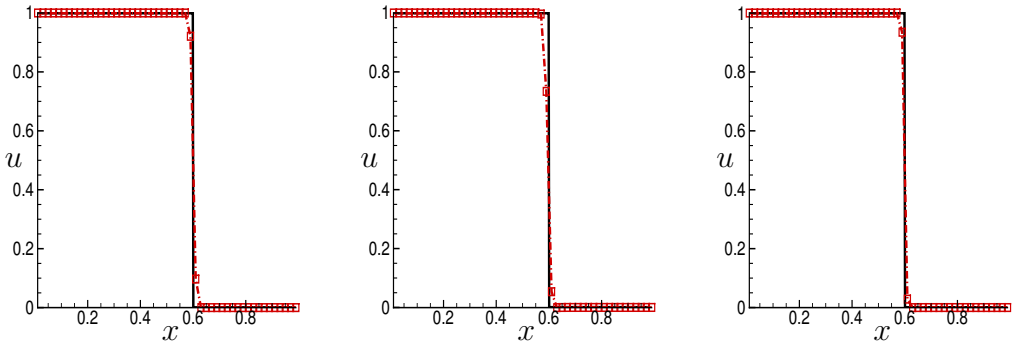

Figure 1: Results of Example 2.2 by the anti-diffusive WENO5/SR with $N = 50$ at $t = 0.3$. Solid line: exact solution; dashed line with symbols: computed solution. Left: $\mu = 10$, CFL=0.5; middle: $\mu = 800$, CFL=0.5; right: $\mu = 10000$, CFL=0.2.

scheme, we test for the cases of $\mu = 10$, $\mu = 800$ and $\mu = 10000$ with the same mesh $N = 50$ at a final time $t = 0.3$. In the case of $\mu = 10$, both schemes can capture the discontinuity at the correct position (see the left subplots of Figs. 1 and 2). For the stiffer case where $\mu = 800$, the propagation speed of the discontinuity computed by splitting WENO5 is qualitatively slower than the analytical value as shown by the middle subplot of Fig. 2, whereas at $\mu = 10000$, the discontinuity solved by splitting WENO5 does not move at all. If the mesh is sufficiently refined, the splitting WENO5 can capture the correct solution. However, for this example in the case where $\mu = 10000$, at least $N = 3000$ points are needed.

We also note that the anti-diffusive WENO/SR is able to produce correct results with a standard CFL number. Even in the very stiff case $\mu = 10000$, CFL=0.2 can be used. But the splitting WENO5 needs a very small CFL number (e.g., CFL=0.05) for stability.

Remark 2.4. *In this example, we also show the results by the standard WENO5 without splitting in Fig. 3. It produces similar spurious waves as the splitting WENO5 with the same mesh size, but it requires a smaller CFL number. From now on the numerical results by the proposed scheme are only compared with the results by splitting WENO5. The results by standard WENO5 without splitting will not be shown in the remaining examples.*

Example 2.3. 1D scalar test case of a nonlinear $f(u)$.

Consider a nonlinear problem (4) with $f(u) = \frac{u^2}{2} + u$, $S(u)$ in (5) and $\alpha = 0.5$. The initial condition is (6). The discontinuity has a speed of $\frac{3}{2}$.

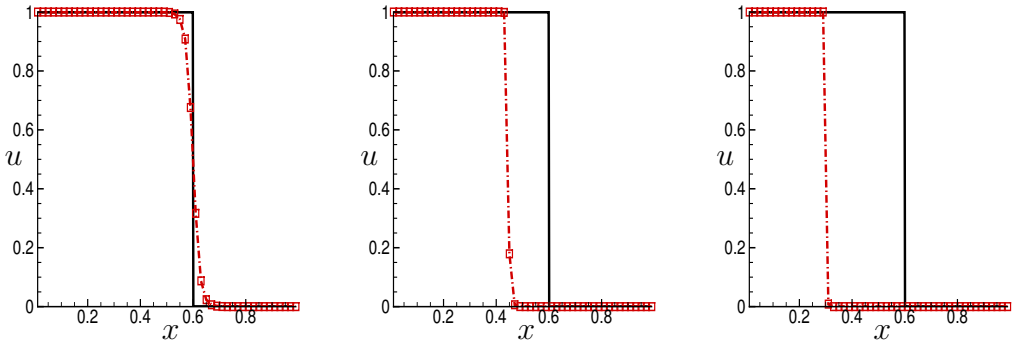

Figure 2: Results of Example 2.2 by the splitting WENO5 scheme with $N = 50$ at $t = 0.3$. Solid line: exact solution; dashed line with symbols: computed solution. Left: $\mu = 10$, CFL=0.5; middle: $\mu = 800$, CFL=0.1; right: $\mu = 10000$, CFL=0.05.

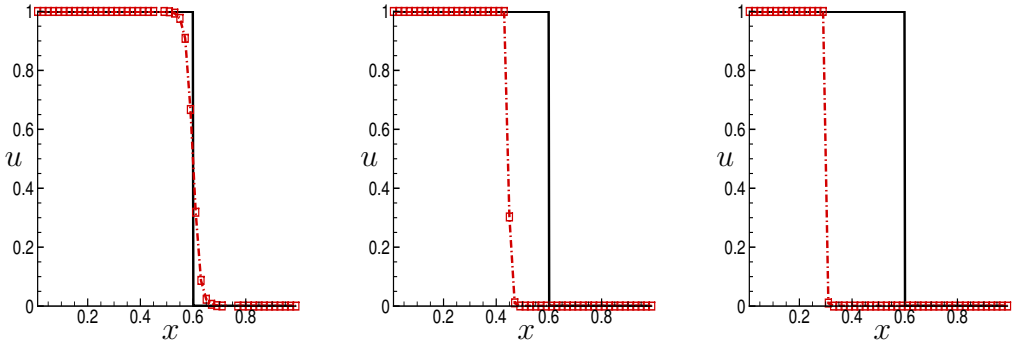

Figure 3: Results of Example 2.2 by the standard WENO5 without splitting scheme with $N = 50$ at $t = 0.3$. Solid line: exact solution; dashed line with symbols: computed solution. Left: $\mu = 10$, CFL=0.5; middle: $\mu = 800$, CFL=0.1; right: $\mu = 10000$, CFL=0.02.

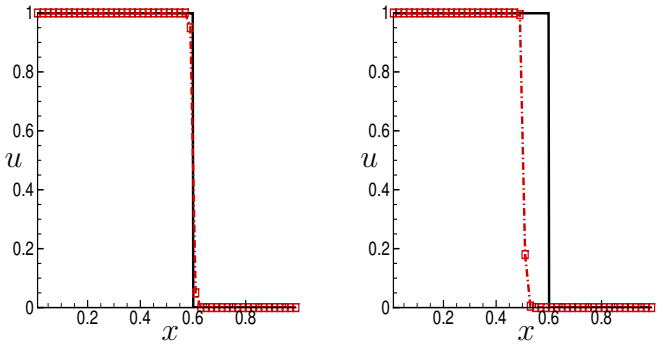

Figure 4: Results of Example 2.3 by different WENO schemes for $\mu = 1000$ with $N = 50$ at $t = 0.2$. Solid line: exact solution; dashed line with symbols: left: anti-diffusive WENO5/SR with CFL=0.2; right: splitting WENO5 with CFL=0.2.

We run the numerical experiment to $t = 0.2$ so that the exact solution is the same as in Example 1. The discontinuity moves to $x = 0.6$ at $t = 0.2$. We plot the results obtained by the anti-diffusive WENO5/SR and splitting WENO5 schemes in the left subplot and right subplot of Fig. 4. Again $N = 50$ and CFL=0.2 are used. Only the anti-diffusive WENO5/SR gives the correct numerical result (see the left subplot of Fig. 4) whereas the splitting WENO5 scheme fails to produce the correct shock speed in the underresolved mesh.

The result with the stiff cubic nonlinear source term (5) studied by LeVeque and Yee can be found in [22, 21]. The cubic nonlinearity case is slightly more complicated as one or more standing wave numerical solutions can be obtained, depending on the sign of μ and the shock-capturing method [22, 21].

3 Extension to 2D scalar problems

It is straightforward to extend the proposed method to the two-dimensional scalar case. Consider the two-dimensional scalar hyperbolic conservation law with stiff reaction term

$$u_t + f(u)_x + g(u)_y = S(u), \tag{35}$$

where $S(u)$ is the same as (5), i.e., $S(u) = -\mu u\,(u-\alpha)\,(u-1)$, $(0 < \alpha < 1)$, with piecewise constant initial condition

$$u(x,y,0) = \begin{cases} 1, & (x,y) \in \Omega_0 \subset \mathbb{R}^2, \\ 0, & (x,y) \in \mathbb{R}^2 \setminus \Omega_0, \end{cases} \tag{36}$$

where Ω_0 is a given domain in $\mathbb{R}^2$.

We again use the splitting method

$$u^{n+1} = A\left(\frac{\Delta t}{2}\right) R(\Delta t) A\left(\frac{\Delta t}{2}\right) u^n, \tag{37}$$

with the anti-diffusive WENO5 as the convection operator and the linearized trapezoidal method (31) as the ODE solver in the reaction step.

Let $I_{ij} = [x_{i-\frac{1}{2}}, x_{i+\frac{1}{2}}] \times [y_{j-\frac{1}{2}}, y_{j+\frac{1}{2}}], i = 1, \ldots, N_x, j = 1, \ldots, N_y$ be a uniform partition of the two-dimensional computational domain, with the grid points $x_i = \frac{1}{2}(x_{i-\frac{1}{2}} + x_{i+\frac{1}{2}})$ and $y_j = \frac{1}{2}(y_{j-\frac{1}{2}} + y_{j+\frac{1}{2}})$. Let u_{ij}^n be the approximated solution at (x_i, y_j, t_n), $i = 1, \ldots, N_x$, $j = 1, \ldots, N_y$. We apply the subcell resolution procedure in the reaction step dimension by dimension in the two-dimensional case.

(1) Identify the transition points by the shock indicator in both x- and y-directions.

Define the cell I_{ij} as troubled in the x-direction if $|s_{ij}^x| \geq |s_{i-1,j}^x|$ and $|s_{ij}^x| \geq |s_{i+1,j}^x|$ with at least one strict inequality where

$$s_{ij}^x = \text{minmod}\{u_{i+1,j} - u_{ij}, u_{ij} - u_{i-1,j}\}. \tag{38}$$

Similarly we can define the cell I_{ij} as troubled in the y-direction if $|s_{ij}^y| \geq |s_{i,j-1}^y|$ and $|s_{ij}^y| \geq |s_{i,j+1}^y|$ with at least one strict inequality where

$$s_{ij}^y = \text{minmod}\{u_{i,j+1} - u_{ij}, u_{ij} - u_{i,j-1}\}. \tag{39}$$

If I_{ij} is only troubled in one direction, we apply the subcell resolution along this direction. If I_{ij} is troubled in both directions, we choose the direction which has a larger jump. Namely, if $|s_{ij}^x| \geq |s_{ij}^y|$, subcell resolution is applied along the x-direction, otherwise it is done along the y-direction.

In the following steps (2)-(3), without loss of generality, we assume the subcell resolution is applied in the x-direction.

(2) Modify the point value u_{ij} in the troubled cell I_{ij} by

$$\tilde{u}_{ij} = \begin{cases} p_{i-s,j}(x_i), & \theta \geq x_i \\ p_{i+r,j}(x_i), & \theta < x_i \end{cases}, \tag{40}$$

where the location θ is determined by conservation

$$\int_{x_{i-1/2}}^{\theta} p_{i-s,j}(x)dx + \int_{\theta}^{x_{i+1/2}} p_{i+r,j}(x)dx = u_{ij}\,\Delta x. \tag{41}$$

The treatment of the situation where θ satisfying (41) does not exist is the same as in the 1D case.

(3) Use $\tilde{u}_{ij}$ instead of u_{ij} in the ODE solver if the cell I_{ij} is a troubled cell, i.e.,

$$u_{ij}^{n+1} = u_{ij}^n + \frac{\Delta t S(\tilde{u}_{ij})}{1 - \frac{\Delta t}{2} S'(\tilde{u}_{ij})}. \tag{42}$$

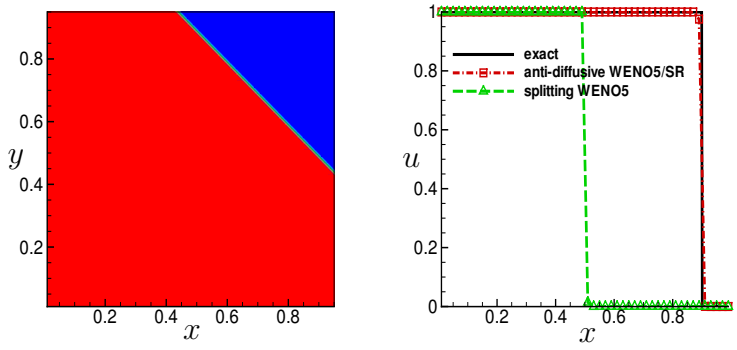

Figure 5: Results of Example 3.1 by the anti-diffusive WENO5/SR scheme: $\mu = 10^4$, $t = 0.2$, $N = 50$, CFL=0.1. Left: 2D contour; right: 1D cross section at $y = 0.5$.

3.1 Numerical examples of 2D scalar problems

Example 3.1. 2D scalar test case of linear fluxes.

Consider Eq. (35) with $f(u) = g(u) = u$ on the domain $[0, 1]^2$, the initial condition is taken as

$$u(x, y, 0) = \begin{cases} 1, & x + y \leq 1, \\ 0, & x + y > 1. \end{cases} \tag{43}$$

Initially the discontinuity is located on the diagonal of the square domain. It moves at a speed $\sqrt{2}$ in the 45° direction. The segments $x = 0$ and $y = 0$ are subject to the inflow boundary condition and the other two sides are subject to the outflow boundary condition.

A stiff case $\mu = 10^4$ at time $t = 0.2$ is considered. The left subplot of Fig. 5 shows 2D contour of the anti-diffusive WENO5/SR with a coarse 50×50 mesh and CFL=0.1. The right subplot shows a comparison between the anti-diffusive WENO5/SR with the splitting WENO5 using the same mesh at $y = 0.5$. At $t = 0.2$, the discontinuity moves to $x = 0.9$. The proposed method is able to capture the correct location of the discontinuity with a very coarse mesh. However, the splitting WENO5 scheme fails to produce the correct shock speed on this underresolved mesh.

Example 3.2. 2D scalar test case of nonlinear fluxes.

In the second example, we consider a nonlinear problem Eq. (35) with $f(u) = g(u) = \frac{u^2}{2}$ on the domain $[0, 1]^2$ with the same initial condition (43). The boundary conditions are the same as in Example 3.1. In this example, the discontinuity moves at a speed $1/\sqrt{2}$. A more stiff case $\mu = 10^5$ is tested. The left subplot of Fig. 6 shows the 2D contour results by the anti-diffusive WENO5/SR scheme with a coarse 50×50 mesh and CFL=0.1. The right subplot shows the 1D cross section at $y = 0.5$ by the anti-diffusive

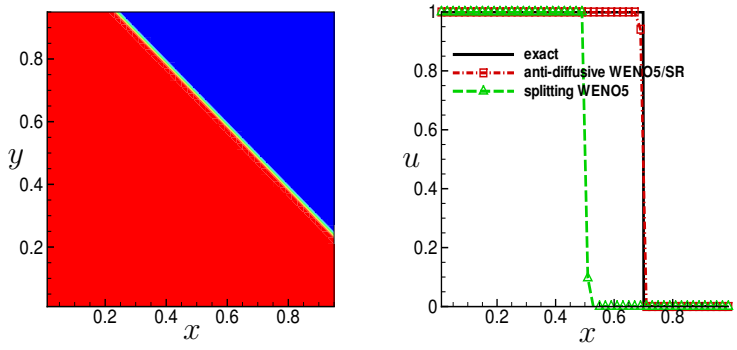

Figure 6: Results of Example 2.3 by the anti-diffusive WENO5/SR scheme: $\mu = 10^5$, $t = 0.2$, $N = 50$, CFL=0.1. Left: 2D contour; right: 1D cross section at $y = 0.5$.

WENO5/SR and the splitting WENO5 with the exact solution at $t = 0.2$ where the discontinuity moves to $x = 0.7$. The numerical solution by the proposed scheme has very good agreement with the exact solution, but the discontinuity solved with the splitting WENO5 does not move.

4 Extension to 1D reactive Euler equations

In this section, we extend our approach to the reactive Euler equations. Consider the simplest one-dimensional reactive Euler equation with only two chemical states: burnt gas and unburnt gas. The unburnt gas is converted to burnt gas via a single irreversible reaction. Without heat conduction and viscosity, the system can be written as

$$\begin{aligned} \rho_t + (\rho u)_x &= 0, && (44)\\ (\rho u)_t + (\rho u^2 + p)_x &= 0, && (45)\\ E_t + (u(E+p))_x &= 0, && (46)\\ (\rho z)_t + (\rho u z)_x &= -K(T)\rho z, && (47) \end{aligned}$$

where ρ is the mixture density, u is the mixture velocity, E is the mixture total energy per unit volume, p is the pressure, z is the mass fraction of the unburnt gas, K is the chemical reaction rate and T is the temperature. The pressure is given by

$$p = (\gamma - 1)(E - \frac{1}{2}\rho u^2 - q_0 \rho z), \tag{48}$$

where q_0 is the chemical heat released in the reaction. The temperature is defined as

$$T = \frac{p}{\rho}. \tag{49}$$

The reaction rate $K(T)$ is modeled by an Arrhenius law

$$K(T) = K_0 \exp\left(\frac{-T_{ign}}{T}\right), \tag{50}$$

where K_0 is the reaction rate constant and T_{ign} is the ignition temperature. The reaction rate may be also modeled in the Heaviside form

$$K(T) = \begin{cases} 1/\varepsilon & T \geq T_{ign} \\ 0 & T < T_{ign} \end{cases}, \tag{51}$$

where ε is the reaction time and $1/\varepsilon$ is roughly equal to K_0.

We treat (44)-(47) similarly as the scalar case.

4.1 Convection operator

In the scalar problem Eq. (4), we have applied the anti-diffusive WENO5 scheme as the convection operator because the discontinuous wave is a contact discontinuity. However, the Chapman-Jouguet (C-J) detonation wave is a shock followed by a reaction. In general, it is not safe to apply the anti-diffusive technique to a shock, since it may generate an entropy-violating solution. Therefore, we do not apply the anti-diffusive sharpening procedure here. This is not a problem because the standard WENO5 scheme is already able to capture the shock very sharply (better than its capability to capture contact discontinuities). In the system case, we use WENO5 with Lax-Friedrichs flux splitting (WENO-LF) and the local characteristic decomposition with RK3 in time discretization as the convection operator in the reactive Euler problems. We refer to [19] for more details of this algorithm.

4.2 Reaction operator

The reaction step for the system case is slightly different from the scalar case because there are more component variables (ρz and T) involved in the source term. The key point here is to identify transition points correctly and to extrapolate the variables ρz and T.

(1) To apply step (1) in Section 2.2, we need to choose one variable to examine. Note that in a detonation wave, the pressure, temperature, and density all have a reaction zone (like an "overshoot") and a shock zone. Only the mass fraction z has a clean single shock wave. This can be seen from the mass fraction equation. Eliminating the density from Eq. (47) by using Eq. (44), we obtain

$$z_t + u z_x = -K(T) z, \tag{52}$$

which is of the scalar type Eq. (4). This helps us identify transition points by the variable z. Define the cell I_i as troubled if $|s_i| \geq |s_{i-1}|$ and $|s_i| \geq |s_{i+1}|$ (with at least one strict inequality) where

$$s_i = \text{minmod}\{z_{i+1} - z_i, z_i - z_{i-1}\}. \tag{53}$$

(2) After a troubled cell I_i is identified, first find the shock location θ by solving the conservation Eq. (28) with the variable u taken as the total energy E

$$\int_{x_{i-1/2}}^{\theta} p_{i-s}(x; E)dx + \int_{\theta}^{x_{i+1/2}} p_{i+r}(x; E)dx = E_i \, \Delta x, \tag{54}$$

where the ENO interpolation polynomials $p_i(x; E)$ are computed based on values of E. The energy E is chosen because it is a conserved variable. We assume the shock locations are the same for all variables. Then we extrapolate the variables ρ, z and T separately. The new mass fraction $\tilde{z}$, temperature $\tilde{T}$ and density $\tilde{\rho}$ are obtained from the ENO interpolation polynomials

$$\begin{cases} \tilde{z}_i = p_{i-s}(x_i; z), \quad \tilde{T}_i = p_{i-s}(x_i; T), \quad \tilde{\rho}_i = p_{i-s}(x_i; \rho), \quad \text{if } \theta \geq x_i \\ \tilde{z}_i = p_{i+r}(x_i; z), \quad \tilde{T}_i = p_{i+r}(x_i; T), \quad \tilde{\rho}_i = p_{i+r}(x_i; \rho), \quad \text{if } \theta < x_i \end{cases}. \tag{55}$$

Remark 4.1. *$s = r = 1$ works well in all the numerical examples for the system case.*

Remark 4.2. *Observe that the mass fraction z has values 0 or 1 for the burnt gas and unburnt gas, respectively. Values between 0 and 1 denote the gas changing from unburnt to burnt. However, in stiff reaction problems, the reaction is very fast and the reaction zone is much smaller than the grid size for an underresolved mesh. Thus in stiff reaction problems, the grid values of z can be simplified to have only two values 0 and 1, but no middle values, i.e.,*

$$\tilde{z}_i = \begin{cases} 0, & \theta \geq x_i \\ 1, & \theta < x_i \end{cases} \tag{56}$$

instead of the values obtained from the ENO polynomial extrapolation.

(3) For simplicity, we use the explicit Euler method as the ODE solver in the reaction step

$$(\rho z)_i^{n+1} = (\rho z)_i^n + \Delta t S(\tilde{T}_i, \tilde{\rho}_i, \tilde{z}_i). \tag{57}$$

In general, a regular CFL=0.1 can be used in the proposed scheme to produce a stable solution. But the solution is very coarse in the reaction zone because of the underresolved mesh in time. In order to obtain more accurate results in the reaction zone, we evolve one reaction step via N_r sub steps, i.e.,

$$u^{n+1} = A\left(\frac{\Delta t}{2}\right) R\left(\frac{\Delta t}{N_r}\right) \cdots R\left(\frac{\Delta t}{N_r}\right) A\left(\frac{\Delta t}{2}\right) u^n \tag{58}$$

in some numerical examples.

4.3 Numerical examples of one-dimensional detonation waves

In this section, we test the proposed method on five examples of one-dimensional detonation waves. The first example uses the Arrhenius law (50). The next four examples are based on the Heaviside model. The proposed method uses a fifth-order WENO-LF with RK3 as the convection operator, and an explicit Euler based on the subcell resolution as the reaction operator.

Example 4.1. C-J detonation wave (Arrhenius case).

The first example uses the Arrhenius source term (50) and has been studied in [17, 33]. The initial values consist of totally burnt gas on the left-hand side and totally unburnt gas on the right-hand side. The density, velocity, and pressure of the unburnt gas are given by $\rho_u = 1$, $u_u = 0$ and $p_u = 1$. The heat release $q_0 = 25$ and the ratio of specific heats is set to $\gamma = 1.4$. We consider the ignition temperature $T_{ign} = 25$ and $K_0 = 164180$. We can obtain the C-J initial state for the unburnt gas by, for example, [12]

$$
\begin{aligned}
p_b &= -b + (b^2 - c)^{1/2}, && (59)\\
\rho_b &= \frac{\rho_u[p_b(\gamma+1) - p_u]}{\gamma p_b}, && (60)\\
s_{CJ} &= [\rho_u u_u + (\gamma p_b \rho_b)^{1/2}]/\rho_u, && (61)\\
u_b &= s_{CJ} - (\gamma p_b/\rho_b)^{1/2}, && (62)
\end{aligned}
$$

where

$$
\begin{aligned}
b &= -p_u - \rho_u q_0(\gamma - 1),\\
c &= p_u^2 + 2(\gamma - 1)p_u\rho_u q_0/(\gamma + 1),
\end{aligned}
$$

and s_{CJ} is the speed of the C-J detonation wave. In this example, $S_{CJ} = 7.1247$.

The computational domain is $[0, 30]$. Initially, the discontinuity is located at $x = 10$. At time $t = 1.8$, the detonation wave has moved to $x = 22.8$. The reference solution is computed by the standard WENO5 scheme with $N = 10000$ ($\Delta x = 0.003$), CFL=0.05.

Figures 7-10 show the pressure, temperature, density and mass fraction comparison results between WENO5/SR method with the splitting WENO5 method. Only $N = 50$ ($\Delta x = 0.6$) and CFL=0.1 are used in WENO5/SR. Clearly, our WENO5/SR method is able to capture the correct propagation speed of the detonation wave with this coarse mesh, while the splitting WENO5 with a much finer mesh $N = 300$ produces spurious numerical results. There are small downstream dents located around $x = 8$ and $x = 16$ in Figs. 7-9 which are standard numerical artifacts resulting from a start-up error when a sharp shock, which is not a traveling wave solution of the scheme, is used as an initial condition. These dents become smaller as the mesh refines and will move out of the computational domain after a period of time.

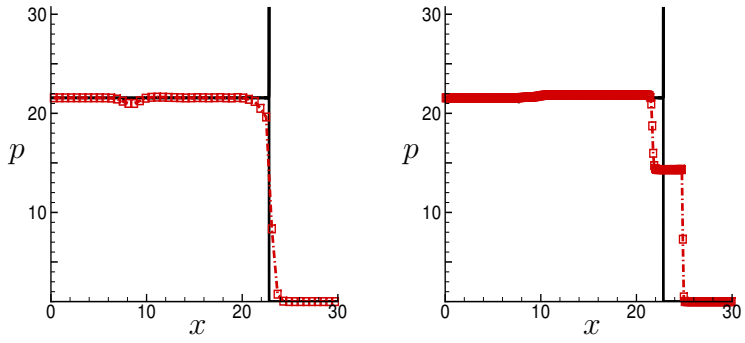

Figure 7: Computed pressure for the Arrhenius Example 4.1 at $t = 1.8$. Solid line: reference solution. Dashed line with symbols: numerical solution. Left: WENO5/SR with $N = 50$, CFL=0.1; right: splitting WENO5 with $N = 300$, CFL=0.1.

We remark that our method can use fewer points than the previous methods in [17] and [33] to obtain similar results. The reason may be due to the high order accuracy of the spatial scheme in the convection step.

Example 4.2. C-J detonation wave (Heaviside case).

In this example the chemical reaction is modeled by the Heaviside form. This example is taken from [13, 5, 2].

Consider the following parameter values in CGS units:

$$\gamma = 1.4, \quad q_0 = 0.5196 \times 10^{10}, \quad \frac{1}{\varepsilon} = 0.5825 \times 10^{10}, \quad T_{ign} = 0.1155 \times 10^{10}.$$

The computational domain is $[0, 0.05]$. The initial conditions are given by

$$(\rho, u, p, z) = \begin{cases} (\rho_b, u_b, p_b, 0) & x \le 0.005 \\ (1.201 \times 10^{-3}, 0, 8.321 \times 10^5, 1) & x > 0.005 \end{cases}, \tag{63}$$

where ρ_b, u_b and p_b are computed by Eqs. (59)-(62). From Eq. (61), the speed of the detonation wave in this example is $D_{CJ} = 1.088 \times 10^5$. In this example, the width of the reaction zone is approximately 5×10^{-5} (see [5] and [13]).

The reference solution is computed by the standard WENO5 scheme with $N = 5000$ points ($\Delta x = 10^{-5}$) and CFL=0.05. The solutions are run to time $t = 3 \times 10^{-7}$. The wave moves to $x = 0.03764$. The pressure, temperature, density and mass fraction results are plotted in Figs. 11-14. $N = 50$ and CFL=0.1 are used in WENO/SR. In this example, 10 sub reaction steps are involved in each time step evolution in order to produce more accurate results in the reaction zone.

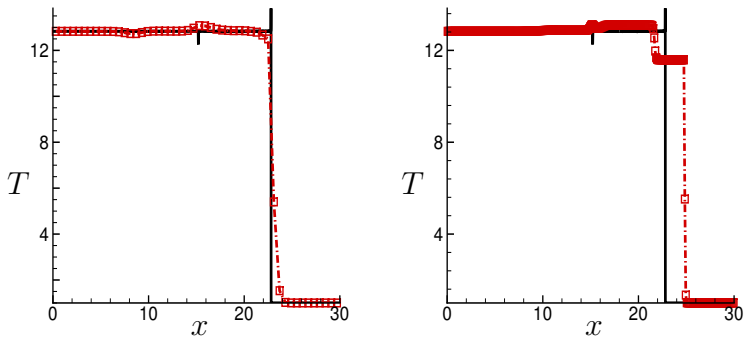

Figure 8: Computed temperature for the Arrhenius Example 4.1 at $t = 1.8$. Solid line: reference solution. Dashed line with symbols: numerical solution. Left: WENO5/SR with $N = 50$, CFL=0.1; right: splitting WENO5 with $N = 300$, CFL=0.1.

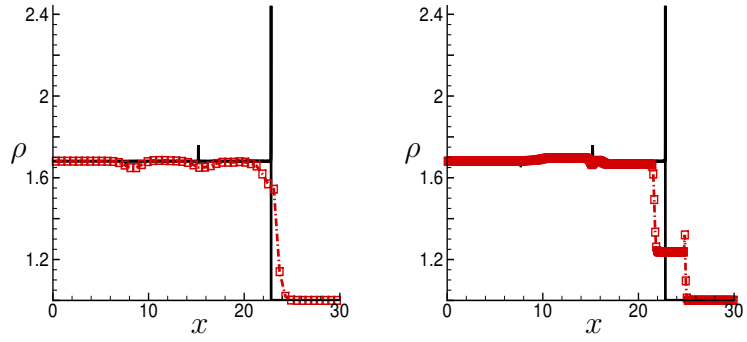

Figure 9: Computed density for the Arrhenius Example 4.1 at $t = 1.8$. Solid line: reference solution. Dashed line with symbols: numerical solution. Left: WENO5/SR with $N = 50$, CFL=0.1; right: splitting WENO5 with $N = 300$, CFL=0.1.

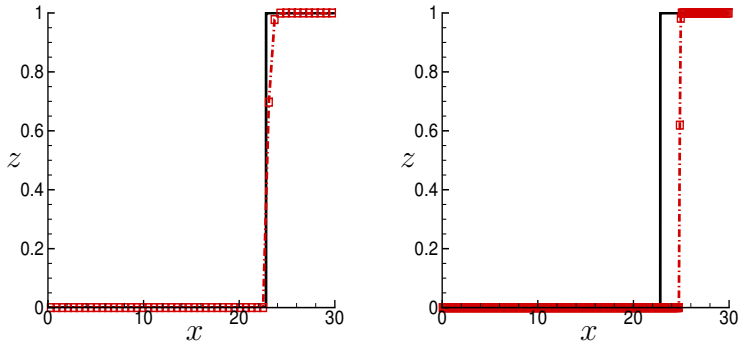

Figure 10: Computed mass fraction for the Arrhenius Example 4.1 at $t = 1.8$. Solid line: reference solution. Dashed line with symbols: numerical solution. Left: WENO5/SR with $N = 50$, CFL=0.1; right: splitting WENO5 with $N = 300$, CFL=0.1.

Again we compare the results by WENO5/SR (left subplots) with splitting WENO5 (right subplots). We can see WENO5/SR with $N = 50$ is able to capture the correct detonation speed. However, splitting WENO5 with $N = 300$ still produces wrong numerical results no matter how small the time step is (the results with smaller time steps are not shown here to save space).

Example 4.3. A strong detonation (Heaviside case).

Here is another detonation problem which is also from [2]. The computational domain is [0,0.05]. The initial data are

$$(\rho, u, p, z) = \begin{cases} (\rho_l, u_l, p_l, 0) & x \le 0.005 \\ (\rho_r, u_r, p_r, 1) & x > 0.005 \end{cases} \tag{64}$$

where $u_l = 9.162 \times 10^4 > u_b$, $\rho_1 = \rho_b$, $p_1 = p_b$, and the right state is the same as in Example 4.2. The exact solution contains a right-moving strong detonation, a right-moving contact discontinuity and a stationary shock.

The reference solutions are computed by standard WENO5 with $N = 5000$ ($\Delta x = 1 \times 10^{-5}$) and CFL=0.05. We display the numerical results by WENO5/SR with $N = 50$, CFL=0.1 and $N_r = 10$ at $t = 2 \times 10^{-7}$. The pressure, temperature, density and mass fraction results are plotted in the left subplots of Figs. 15-18. We also compute the results by the splitting WENO5 with $N = 50$ and CFL=0.01 in the right subplots of Figs. 15-18. We can see WENO5/SR is able to capture the correct shock speed and other waves in a very coarse mesh. But the splitting WENO5 with the same mesh produce spurious waves.

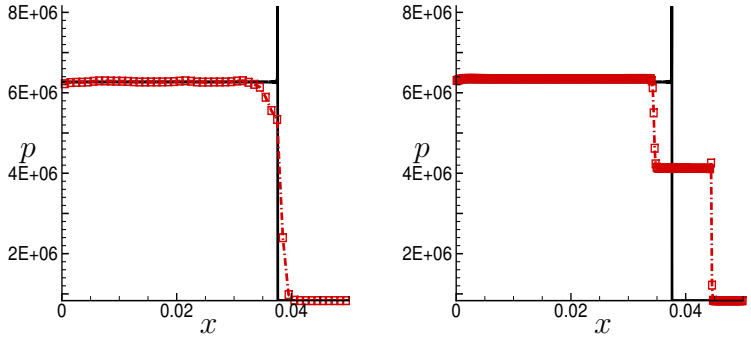

Figure 11: Computed pressure for the Heaviside Example 4.2 at $t = 3 \times 10^{-7}$. Solid line: reference solution. Dashed line with symbols: numerical solution. Left: WENO5/SR with $N = 50$, CFL=0.1, $N_r = 10$; right: splitting WENO5 with $N = 300$, CFL=0.01.

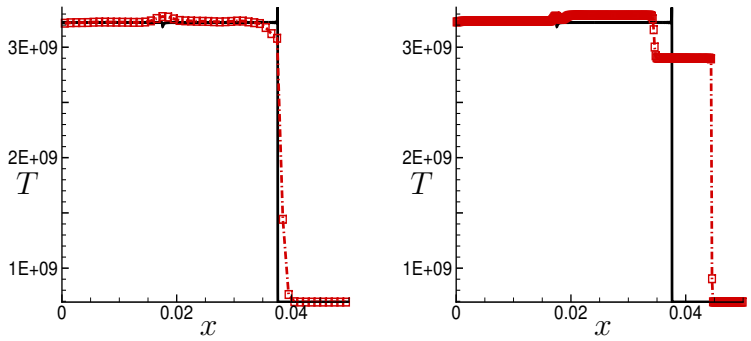

Figure 12: Computed temperature for the Heaviside Example 4.2 at $t = 3 \times 10^{-7}$. Solid line: reference solution. Dashed line with symbols: numerical solution. Left: WENO5/SR with $N = 50$, CFL=0.1, $N_r = 10$; right: splitting WENO5 with $N = 300$, CFL=0.01.

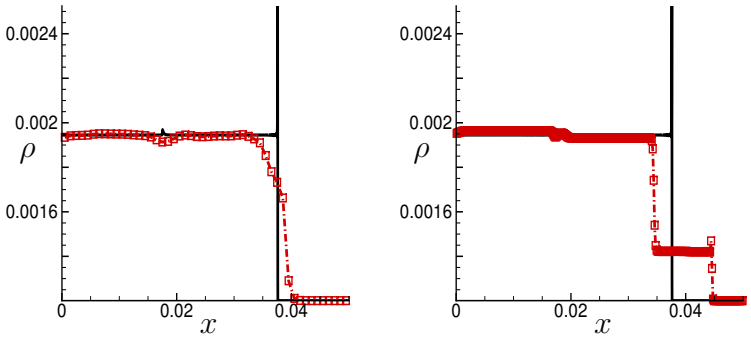

Figure 13: Computed density for the Heaviside Example 4.2 at $t = 3 \times 10^{-7}$. Solid line: reference solution. Dashed line with symbols: numerical solution. Left: WENO5/SR with $N = 50$, CFL=0.1, $N_r = 10$; right: splitting WENO5 with $N = 300$, CFL=0.01.

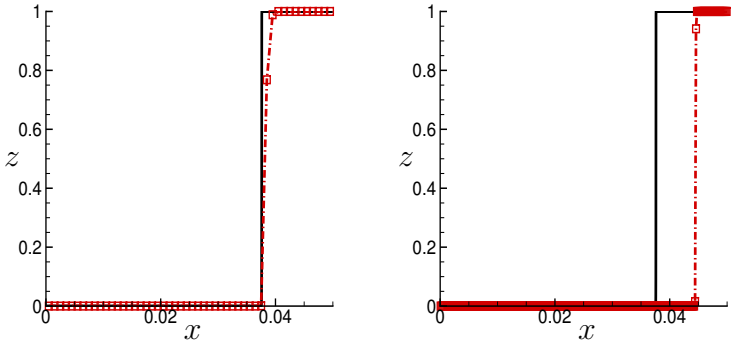

Figure 14: Computed mass fraction for the Heaviside Example 4.2 at $t = 3 \times 10^{-7}$. Solid line: reference solution. Dashed line with symbols: numerical solution. Left: WENO5/SR with $N = 50$, CFL=0.1, $N_r = 10$; right: splitting WENO5 with $N = 300$, CFL=0.01.

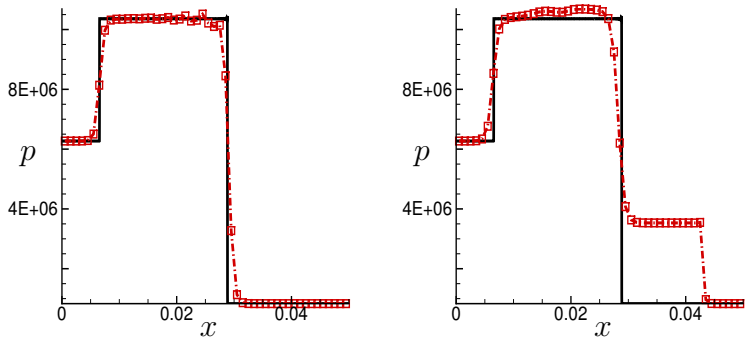

Figure 15: Computed pressure for the Heaviside Example 4.3 at $t = 2 \times 10^{-7}$. Solid line: reference solution. Dashed line with symbols: numerical solution. Left: WENO5/SR with $N = 50$, CFL=0.1, $N_r = 10$; right: splitting WENO5 with $N = 50$, CFL=0.01.

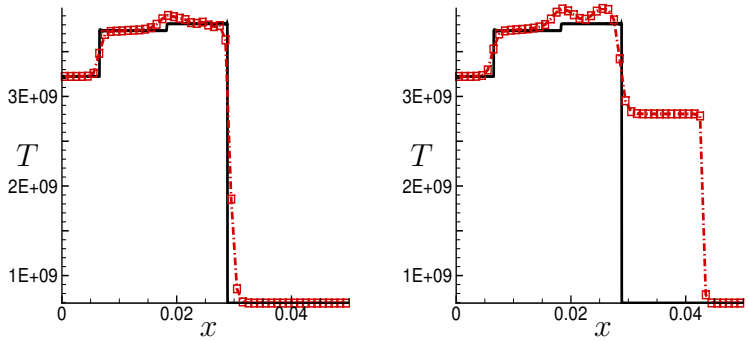

Figure 16: Computed temperature for the Heaviside Example 4.3 at $t = 2 \times 10^{-7}$. Solid line: reference solution. Dashed line with symbols: numerical solution. Left: WENO5/SR with $N = 50$, CFL=0.1, $N_r = 10$; right: splitting WENO5 with $N = 50$, CFL=0.01.

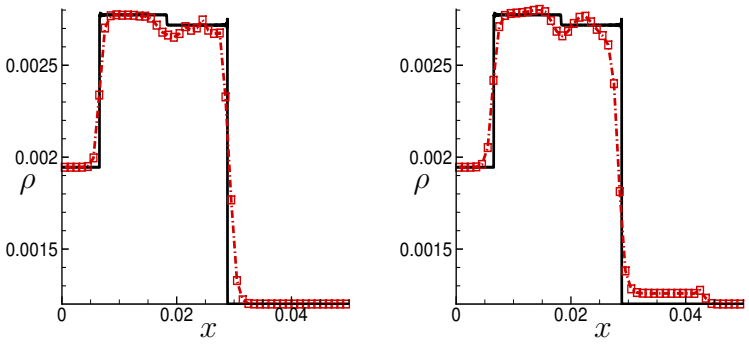

Figure 17: Computed density for the Heaviside Example 4.3 at $t = 2 \times 10^{-7}$. Solid line: reference solution. Dashed line with symbols: numerical solution. Left: WENO5/SR with $N = 50$, CFL=0.1, $N_r = 10$; right: splitting WENO5 WENO5 with $N = 50$, CFL=0.01.

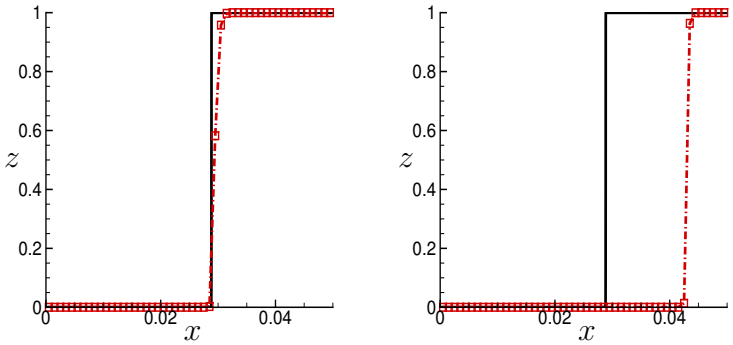

Figure 18: Computed mass fraction for the Heaviside Example 4.3 at $t = 2 \times 10^{-7}$. Solid line: reference solution. Dashed line with symbols: numerical solution. Left: WENO5/SR with $N = 50$, CFL=0.1, $N_r = 10$; right: splitting WENO5 WENO5 with $N = 50$, CFL=0.01.

Example 4.4. Collision of a detonation with a rarefaction wave (Heaviside case).

Next, we consider a one-dimensional detonation problem involving a collision with a rarefaction wave. This example is taken from [3] and [18]. The parameters are taken as $\gamma = 1.2$, $q_0 = 50$, $\frac{1}{\varepsilon} = 230.75$ and $T_{ign} = 3$.

The computational domain is [0,100]. The initial data are

$$(\rho, u, p, z) = \begin{cases} (\rho_l, u_l, p_l, 0) & x \leq 10 \\ (\rho_m, u_m, p_m, 0) & 10 < x \leq 20 \\ (\rho_r, u_r, p_r, 1) & x > 20 \end{cases} \tag{65}$$

where $\rho_l = 2$, $u_l = 4$, $p_l = 40$, $\rho_m = 3.64282$, $p_m = 54.8244$, $u_m = 6.2489$, $\rho_r = 1$, $u_l = 0$ and $p_l = 1$.

The exact solution contains a right-moving strong detonation, a right moving rarefaction wave, a right moving contact discontinuity, and a left moving rarefaction wave. After some time, the right moving rarefaction wave will catch up with the detonation wave. We consider the solutions before the collision of the detonation with the rarefaction at $t = 2$ and the solutions after the collision at $t = 8$. The reference solutions are computed by standard WENO5 with $N = 10,000$ ($\Delta x = 0.01$) and CFL=0.3.

Figure 19 shows pressure, temperature, density and mass fraction results by WENO5/SR with $N = 100$ and CFL=0.1 at $t = 2$. Before the collision, both the WENO5/SR and the splitting WENO5 method can capture the correct shock speed on the mesh with 100 points where the results by the splitting WENO5 are not shown here. However, after the collision at $t = 8$ (see Figs. 20-23), the splitting WENO5 cannot capture the correct shock location and produce spurious numerical waves around the detonation which can be easily seen in pressure, temperature and mass fraction results (see the right subplots of Figs. 20, 21, 23). The spurious waves in the density are smaller, appearing in the bottom corner around the detonation (see the right subplots of Fig. 22). The proposed WENO5/SR scheme is able to capture the correct shock speed and other waves in a very coarse mesh.

Example 4.5. A detonation interacting with an oscillatory profile (Heaviside case).

The last one-dimensional detonation problem involves a collision with an oscillatory profile. This example is also taken from [3]. The parameters γ, q_0 and T_{ign} are the same as Example 4.4 except $\frac{1}{\varepsilon} = 1000$.

The computational domain is $[0, 2\pi]$. The initial data are

$$(\rho, u, p, z) = \begin{cases} (\rho_l, u_l, p_l, 0) & x \leq \frac{\pi}{2} \\ (\rho_r, u_r, p_r, 1) & x > \frac{\pi}{2} \end{cases}, \tag{66}$$

where $\rho_l = 1.79463$, $u_l = 3.0151$, $p_l = 21.53134$, $\rho_r = 1.0 + 0.5 \sin 2x$, $u_l = 0$ and $p_l = 1$.

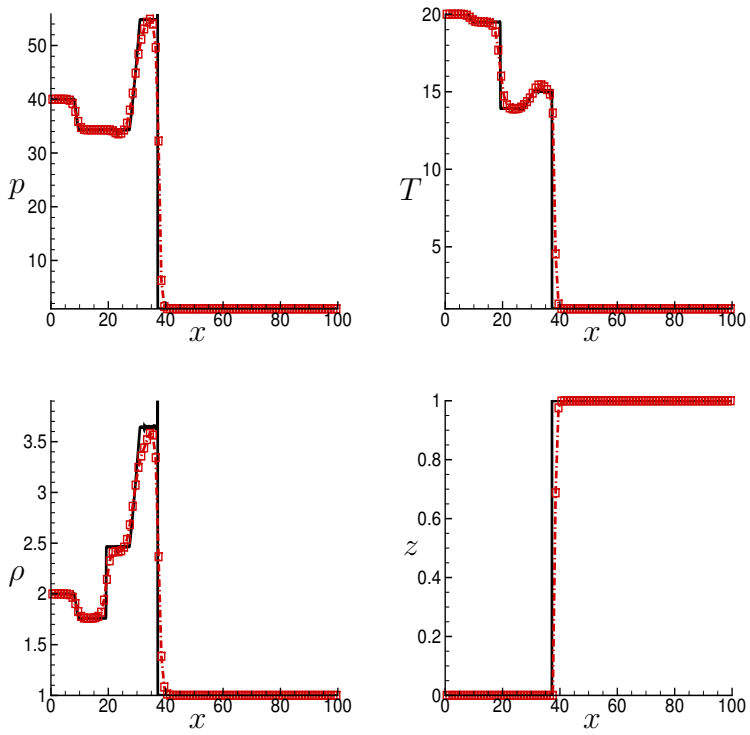

Figure 19: Results for the Heaviside Example 4.4 at $t = 2$. Solid line: reference solution. Dashed line with symbols: numerical solution of WENO5/SR with $N = 100$, CFL=0.1. Top left: pressure; top right: temperature; bottom left: density; bottom right: mass fraction.

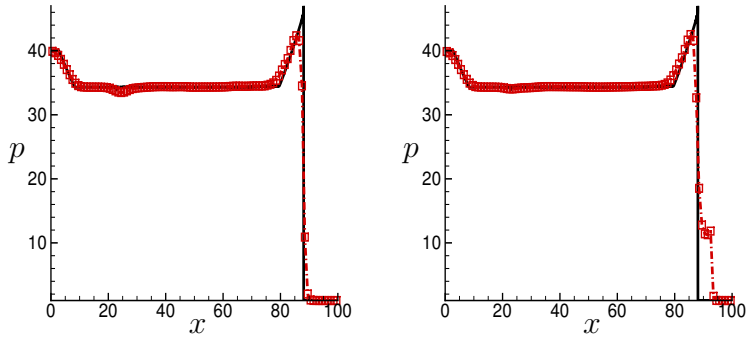

Figure 20: Computed pressure for the Heaviside Example 4.4 at $t = 8$. Solid line: reference solution. Dashed line with symbols: numerical solution. Left: WENO5/SR with $N = 100$, CFL=0.1; right: splitting WENO5 with $N = 100$, CFL=0.1.

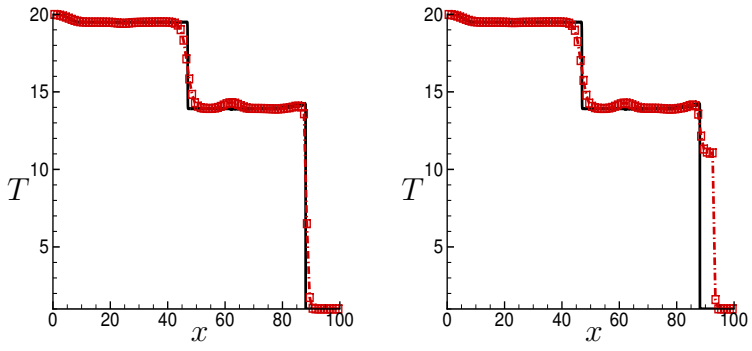

Figure 21: Computed temperature for the Heaviside Example 4.4 at $t = 8$. Solid line: reference solution. Dashed line with symbols: numerical solution. Left: WENO5/SR with $N = 100$, CFL=0.1; right: splitting WENO5 with $N = 100$, CFL=0.1.

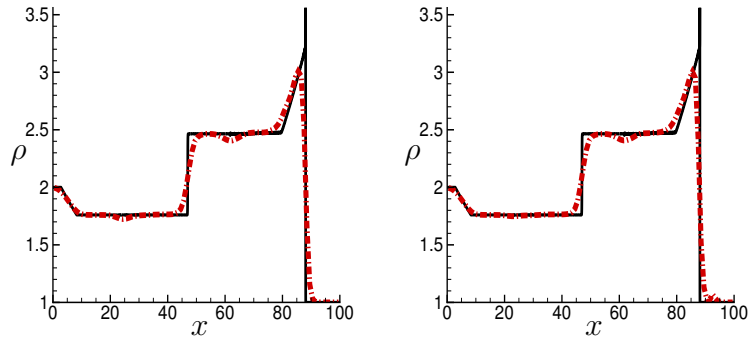

Figure 22: Computed density for the Heaviside Example 4.4 at $t = 8$. Solid line: reference solution. Dashed line: numerical solution. Left: WENO5/SR with $N = 100$, CFL=0.1; right: splitting WENO5 with $N = 100$, CFL=0.1.

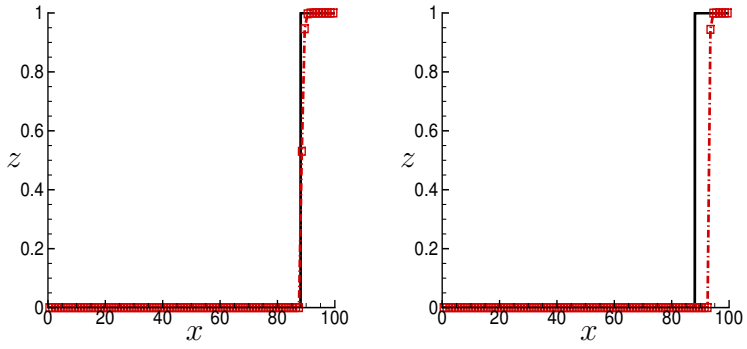

Figure 23: Computed mass fraction for the Heaviside Example 4.4 at $t = 8$. Solid line: reference solution. Dashed line with symbols: numerical solution. Left: WENO5/SR with $N = 100$, CFL=0.1; right: splitting WENO5 with $N = 100$, CFL=0.1.

The reference solutions are computed by splitting WENO5 with $N = 10,000$ and CFL=0.3. The numerically computed pressure, temperature, density and mass fraction at $t = \pi/5$ are plotted in Figs. 24-27 separately, where the left subplots are computed by WENO5/SR with $N = 200$ and CFL=0.1, and the right subplots are computed by splitting WENO5 with $N = 200$ and CFL=0.1. We can see the proposed WENO5/SR is able to handle the interactions between the detonation and the oscillatory wave in a very coarse mesh, while the splitting WENO5 scheme produces unphysical solutions around the detonation shock.

5 Extension to 2D reactive Euler equations

Next, we extend the proposed method to the two-dimensional reactive Euler equations. The considered two-dimensional problem is the extension of the one-dimensional problem, again modeling the reaction with two chemical states and one reaction. The governing equations are

$$\begin{aligned}
\rho_t + (\rho u)_x + (\rho v)_y &= 0 && (67)\\
(\rho u)_t + (\rho u^2 + p)_x + (\rho uv)_y &= 0 && (68)\\
(\rho v)_t + (\rho uv)_x + (\rho v^2 + p)_y &= 0 && (69)\\
E_t + (u(E+p))_x + (v(E+p))_y &= 0 && (70)\\
(\rho z)_t + (\rho uz)_x + (\rho vz)_y &= -K(T)\rho z, && (71)
\end{aligned}$$

where $\rho(x, y, t)$ is the mixture density, $u(x, y, t)$ and $v(x, y, t)$ are the mixture x- and y-velocities, $E(x, y, t)$ is the mixture total energy per unit volume, $p(x, y, t)$ is the pressure,

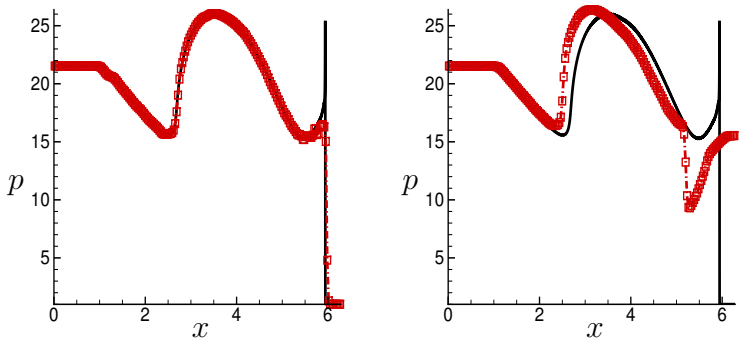

Figure 24: Computed pressure results for the Heaviside Example 4.5 at $t = \pi/5$. Solid line: reference solution. Dashed line with symbols: numerical solution. Left: WENO5/SR with $N = 200$, CFL=0.1; right: splitting WENO5 with $N = 200$, CFL=0.1.

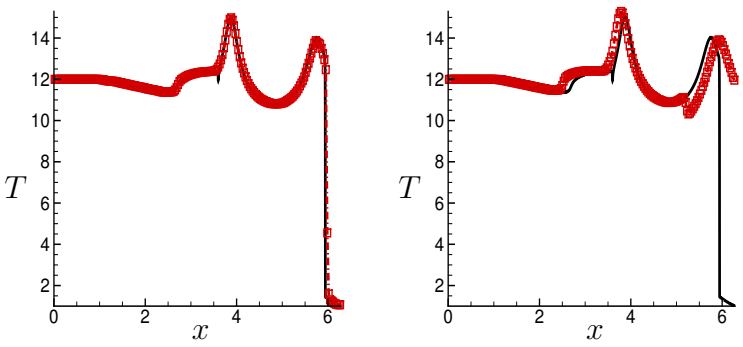

Figure 25: Computed temperature results for the Heaviside Example 4.5 at $t = \pi/5$. Solid line: reference solution. Dashed line with symbols: numerical solution. Left: WENO5/SR with $N = 200$, CFL=0.1; right: splitting WENO5 with $N = 200$, CFL=0.1.

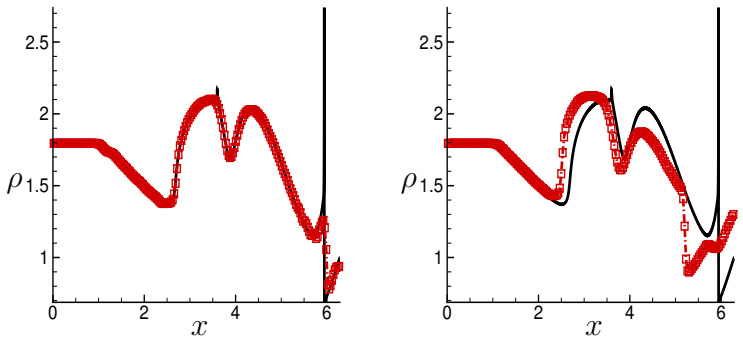

Figure 26: Computed density results for the Heaviside Example 4.5 at $t = \pi/5$. Solid line: reference solution. Dashed line with symbols: numerical solution. Left: WENO5/SR with $N = 200$, CFL=0.1; right: splitting WENO5 with $N = 200$, CFL=0.1.

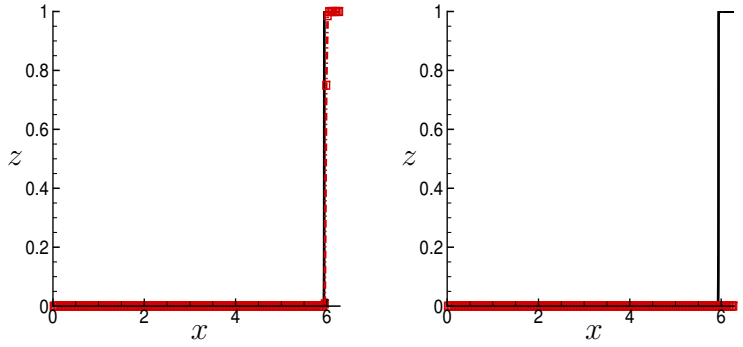

Figure 27: Computed mass fraction results for the Heaviside Example 4.5 at $t = \pi/5$. Solid line: reference solution. Dashed line with symbols: numerical solution. Left: WENO5/SR with $N = 200$, CFL=0.1; right: splitting WENO5 with $N = 200$, CFL=0.1.

$z(x,y,t)$ is the mass fraction of the unburnt gas, $K(T)$ is the chemical reaction rate and $T(x,y,t)$ is the temperature. The pressure is given by

$$p = (\gamma - 1)(E - \frac{1}{2}\rho(u^2 + v^2) - q_0\rho z), \tag{72}$$

where the temperature $T = \frac{p}{\rho}$ and q_0 is the chemical heat released in the reaction. The source term is modeled as in the one-dimensional case. For simplicity, we only consider the Heaviside source term (51).

In the convection step, we use fifth-order WENO-LF with RK3 time discretization.

In the reaction step, we apply the subcell resolution procedure dimension by dimension.

(1) Identify troubled cell I_{ij} in both x- and y-directions by applying the shock indicator to z.

Assuming I_{ij} is troubled in the x-direction, we apply subcell resolution along the x-direction.

(2) Modify the point value z_{ij} T_{ij} and ρ_{ij} in the troubled cell I_{ij} by the ENO interpolation polynomials

$$\begin{cases} \tilde{z}_{ij} = p_{i-s,j}(x_i; z), \quad \tilde{T}_{ij} = p_{i-s,j}(x_i; T), \quad \tilde{\rho}_{ij} = p_{i-s,j}(x_i; \rho), \quad \text{if } \theta \geq x_i \\ \tilde{z}_{ij} = p_{i+r,j}(x_i; z), \quad \tilde{T}_{ij} = p_{i+r,j}(x_i; T), \quad \tilde{\rho}_{ij} = p_{i+r,j}(x_i; \rho), \quad \text{if } \theta < x_i \end{cases}, \tag{73}$$

where the location θ is determined by the conservation of energy E

$$\int_{x_{i-1/2}}^{\theta} p_{i-s,j}(x; E)dx + \int_{\theta}^{x_{i+1/2}} p_{i+r,j}(x; E)dx = E_{ij}\Delta x. \tag{74}$$

For simplicity, in the considered stiff problem, the value of z_{ij} can be taken as

$$\tilde{z}_{ij} = \begin{cases} 0, & \theta \geq x_i \\ 1, & \theta < x_i \end{cases}. \tag{75}$$

(3) For simplicity, explicit Euler is used as the ODE solver.

5.1 Numerical examples of 2D detonation waves

Example 5.1. A 2D detonation wave.

This example is taken from [2]. The chemical reaction is modeled by the Heaviside form with the same parameters q_0, $\frac{1}{\varepsilon}$ and T_{ign} as in Example 4.2. Consider a two-dimensional channel of width 0.005, the upper and lower boundaries are solid walls. The computational domain is $[0, 0.025] \times [0, 0.005]$. The initial conditions are

$$(\rho, u, v, p, z) = \begin{cases} (\rho_l, u_l, 0, p_l, 0), & \text{if } x \leq \xi(y), \\ (\rho_r, u_r, 0, p_r, 1), & \text{if } x > \xi(y), \end{cases} \tag{76}$$

where

$$\xi(y) = \begin{cases} 0.004 & |y - 0.0025| \le 0.001, \\ 0.005 - |y - 0.0025| & |y - 0.0025| < 0.001, \end{cases} \tag{77}$$

and $u_l = 8.162 \times 10^4 > u_b$, $\rho_l = \rho_b$ and $p_l = p_b$. u_b, ρ_b, p_b and the right state are as in Example 4.2.

Similar problems are also computed in [14]. One important feature of this solution is the appearance of triple points, which travel in the transverse direction and reflect from the upper and lower walls. A discussion of the mechanisms driving this solution is given in [20].

Figures 28-29 show density contours computed by WENO5/SR with 500×100 ($\Delta x = \Delta y = 5 \times 10^{-5}$), CFL=0.1 and $N_r = 2$ at eighteen evolutionary times from $t = 0$ to $t = 1.7 \times 10^{-7}$. We can see the movement of the triple points. The same case by WENO5/SR with a much coarser grid 200×40 ($\Delta x = \Delta y = 1.25 \times 10^{-4}$) with CFL=0.1 and $N_r = 2$ at three evolutionary times are shown in Fig. 30. We can see WENO5/SR with the very coarse 200×40 mesh can still capture the correct shock location, although the shocks are smeared due to the lack of resolution. It is more apparent to compare the computed results with the reference solution in a 1D cross section. The reference solutions are computed by standard WENO5 with 2000×400 grid points and CFL=0.3. The results by WENO5/SR and the splitting WENO5 are compared with the same mesh 200×40 and CFL=0.005. Figures 31-34 show the 1D cross section at $y = 0.0025$ at evolutionary times $t = 2 \times 10^{-8}$, $t = 6 \times 10^{-8}$, $t = 1.4 \times 10^{-7}$ and $t = 1.7 \times 10^{-7}$ separately, where the left subplots are computed by WENO5/SR and the right subplots are by splitting WENO5. We can see WENO5/SR has excellent agreement with the reference solutions except it cannot capture the waves sharply due to the underresolved mesh. However the splitting WENO5 method produces spurious waves in front of the detonation shock starting at time $t = 2 \times 10^{-8}$ (right subplot of Fig. 31) and after that the solutions move at a wrong speed (right subplots of Figs. 32-34).

6 Concluding remarks

A new high order finite difference scheme with subcell resolution for hyperbolic conservation laws with stiff source terms has been developed. This method utilizes a fractional step approach with the freedom in choosing any spatial high-resolution shock-capturing schemes and temporal discretizations. In the convection step, any spatial high-resolution scheme can be used. In the reaction step, any explicit ODE solver can be used with the transition points reconstructed by Harten's ENO subcell resolution. The proposed method has high order accuracy in space for smooth flows. It is able to capture the correct discontinuity speed on very coarse meshes and with a reasonable CFL number (If one is interested in resolving the narrow reaction zone at the reaction front, then a

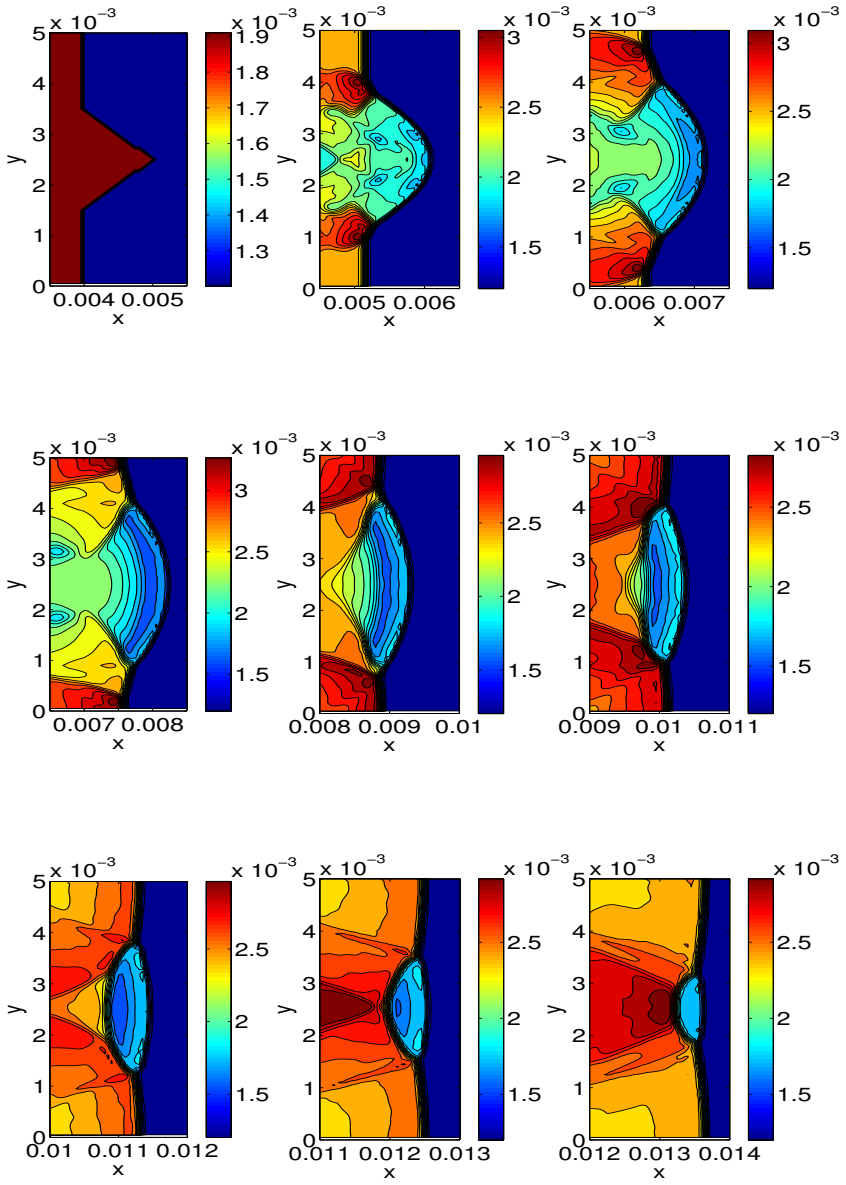

Figure 28: Computed density for Example 5.1: WENO5/SR with 500×100, CFL=0.1 and $N_r = 2$ at nine different evolutionary times $t = 0$, $t = 1 \times 10^{-8}$, $t = 2 \times 10^{-8}$, $t = 3 \times 10^{-8}$, $t = 4 \times 10^{-8}$, $t = 5 \times 10^{-8}$, $t = 6 \times 10^{-8}$, $t = 7 \times 10^{-8}$ and $t = 8 \times 10^{-8}$.

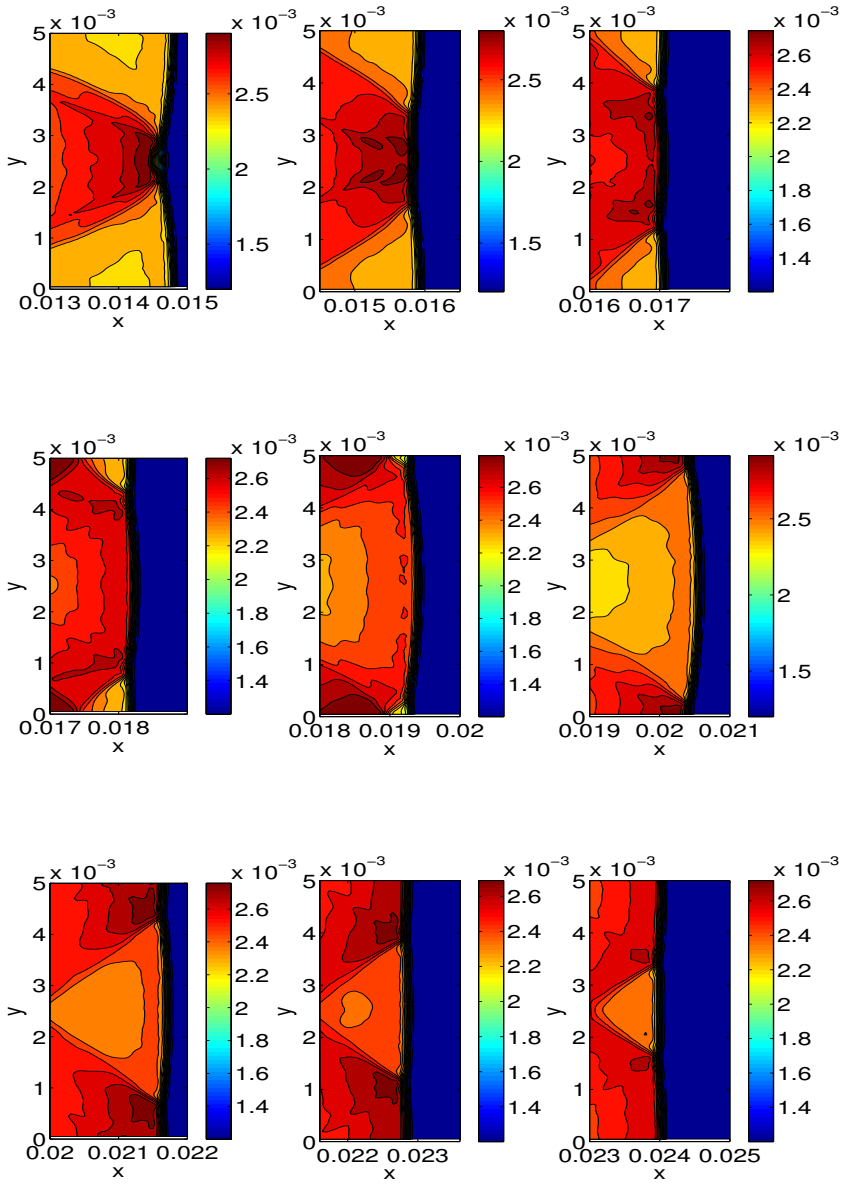

Figure 29: Computed density for Example 5.1: WENO5/SR with 500×100, CFL=0.1 and $N_r = 2$ at nine different evolutionary times $t = 9 \times 10^{-8}$, $t = 1 \times 10^{-7}$, $t = 1.1 \times 10^{-7}$, $t = 1.2 \times 10^{-7}$, $t = 1.3 \times 10^{-7}$, $t = 1.4 \times 10^{-7}$, $t = 1.5 \times 10^{-7}$, $t = 1.6 \times 10^{-7}$ and $t = 1.7 \times 10^{-7}$.

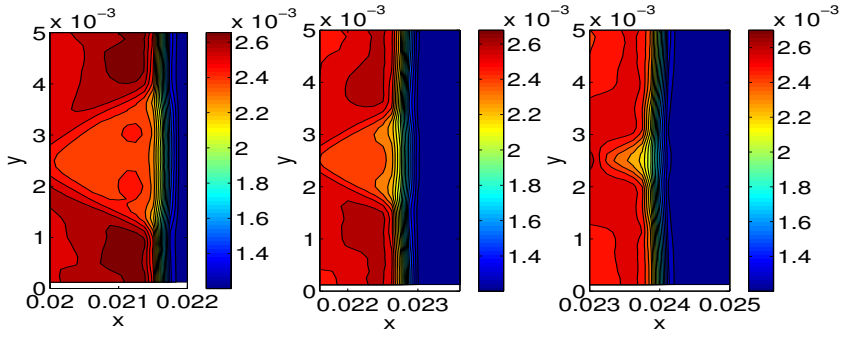

Figure 30: Density results of Example 5.1: WENO5/SR with 200×40, CFL=0.1 and $N_r = 2$ at $t = 1.5 \times 10^{-7}$, $t = 1.6 \times 10^{-7}$ and $t = 1.7 \times 10^{-7}$.

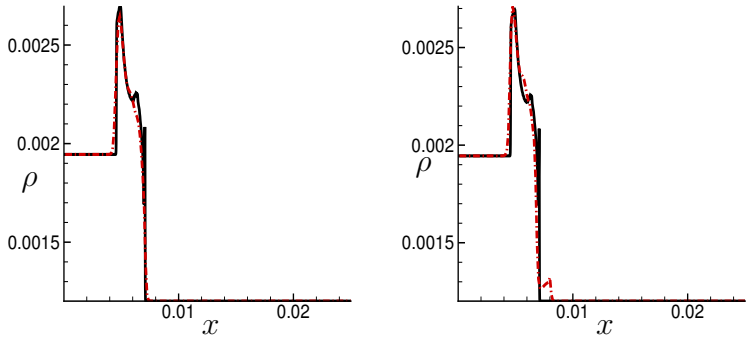

Figure 31: 1D cross-section of Example 5.1 at $t = 2 \times 10^{-8}$ by different WENO schemes with 200×40. Solid line: reference solution; dashed line: numerical solution. Left: WENO5/SR with CFL=0.1, $N_r = 2$; right: splitting WENO5 with CFL=0.05.

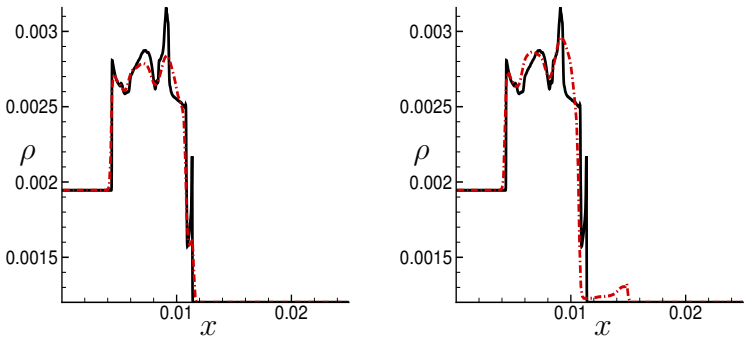

Figure 32: 1D cross-section of Example 5.1 at $t = 6 \times 10^{-8}$ by different WENO schemes with 200×40. Solid line: reference solution; dashed line: numerical solution. Left: WENO5/SR with CFL=0.1, $N_r = 2$; right: splitting WENO5 with CFL=0.05.

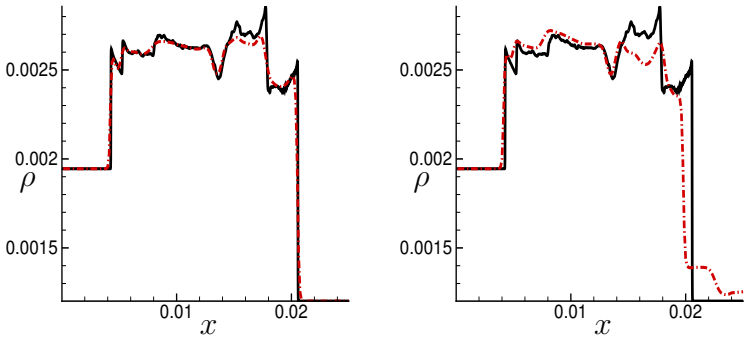

Figure 33: 1D cross-section of Example 5.1 at $t = 1.4 \times 10^{-7}$ by different WENO schemes with 200×40. Solid line: reference solution; dashed line: numerical solution. Left: WENO5/SR with CFL=0.1, $N_r = 2$; right: splitting WENO5 with CFL=0.05.

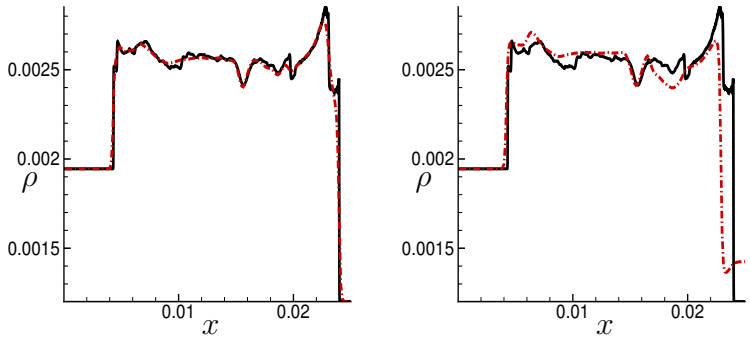

Figure 34: 1D cross-section of Example 5.1 at $t = 1.7 \times 10^{-7}$ by different WENO schemes with 200×40. Solid line: reference solution; dashed line: numerical solution. Left: WENO5/SR with CFL=0.1, $N_r = 2$; right: splitting WENO5 with CFL=0.05.

refined grid resolution is still necessary). It can be used for both stiff and non-stiff problems. Extensive numerical examples for one- and two-dimensional scalar problems and one- and two-dimensional detonation waves demonstrate the robustness of the method.

From the numerical experiments, further containment of numerical dissipation in existing high order shock-capturing schemes can defer the onset of wrong propagation speeds of discontinuities to certain degree. However, the need to contain the spreading of the discontinuity front is the key to overcoming the difficulty. In future work, we will extend this approach to more general chemical reaction models including multiple reaction models.

The current approach is only second order in time due to the splitting method. In the future we will also consider developing a non-splitting method with an explicit RK scheme with the subcell resolution applied to the source term. However this is not a trivial task. Straightforward application of the subcell resolution to the source term in each inner stages of RK scheme does not work. Because in the system case, the source term should choose the correct value for each time step. If there are three inner stages in RK scheme and each stage takes a different value for the source, the convex combination of them may lead to wrong results. We will investigate this in more detail in the future.

Acknowledgments

The authors acknowledge the support of the DOE/SciDAC SAP grant DE-AI02-06ER25796. The work by Bjorn Sjögreen was performed under the auspices of the U.S. Department of Energy at Lawrence Livermore National Laboratory under Contract DE-AC52-07NA27344, LLNL-JRNL-487451. The research of C.-W. Shu is also partially supported

by ARO grant W911NF-08-1-0520. The research of H. C. Yee is also partially supported by the NASA Fundamental Aeronautics Hypersonic program.

References

[1] R. Jeltsch amd P. Klingenstein. Error estimators for the position of discontinuities in hyperbolic conservation laws with source term which are solved using operator splitting. *Comput. Vis. Sci.*, 1:231–249, 1999.

[2] W. Bao and S. Jin. The random projection method for hyperbolic conservation laws with stiff reaction terms. *J. Comput. Phys.*, 163:216–248, 2000.

[3] W. Bao and S. Jin. The random projection method for stiff detonation capturing. *SIAM J. Sci. Comput.*, 23:1000–1025, 2001.

[4] W. Bao and S. Jin. The random projection method for stiff multispecies detonation capturing. *J. Comput. Phys.*, 178:37–57, 2002.

[5] M. Ben-Artzi. The generalized Riemann problem for reactive flows. *J. Comput. Phys.*, 81:70–101, 1989.

[6] A. Berkenbosch, E. Kaasschieter, and R. Klein. Detonation capturing for stiff combustion chemistry. *Combust. Theory Model.*, 2:313–348, 1998.

[7] B. Bihari and D. Schwendeman. Multiresolution schemes for the reactive euler equations. *J. Comput. Phys.*, 154:197–230, 1999.

[8] A. Bourlioux, A. Majda, and V. Roytburd. Theoretical and numerical structure for unstable one-dimensional detonations. *SIAM J. Appl. Math.*, 51:303–343, 1991.

[9] S.-H. Chang. On the application of subcell resolution to conservation laws with stiff source terms. *NASA Technical Memorandum 102384, ICOMP Report 89-27*, 1989.

[10] S.-H. Chang. On the application of subcell resolution to conservation laws with stiff source terms. *NASA Lewis Research Center, Computational Fluid Dynamics Symposium on Aeropropulsion*, pages 215–225, 1991.

[11] A. Chorin. Random choice solution of hyperbolic systems. *J. Comput. Phys.*, 22:517–533, 1976.

[12] A. Chorin. Random choice methods with applications for reacting gas flows. *J. Comput. Phys.*, 25:253–272, 1977.

[13] P. Colella, A. Majda, and V. Roytburd. Theoretical and numerical structure for numerical reacting waves. *SIAM J. Sci. Stat. Comput.*, 7:1059–1080, 1986.

[14] B. Engquist and B. Sjögreen. Robust difference approximations of stiff inviscid detonation waves. *Technical Report CAM 91-03, UCLA.*, 1991.

[15] D. Griffiths, A. Stuart, and H. C. Yee. Numerical wave propagation in an advection equation with a nonlinear source term. *SIAM J. Numer. Anal.*, 29:1244–1260, 1992.

[16] A. Harten. ENO schemes with subcell resolution. *J. Comput. Phys.*, 83:148–184, 1989.

[17] C. Helzel, R. LeVeque, and G. Warneke. A modified fractional step method for the accurate approximation of detonation waves. *SIAM J. Sci. Stat. Comput.*, 22:1489–1510, 1999.

[18] P. Hwang, R. P. Fedkiw, B. Merriman, A. K. Karagozian, and S. J. Osher. Numerical resolution of pulsating detonation waves. *Combust. Theory Model.*, 4:217–240, 2000.

[19] G Jiang and C.-W. Shu. Efficient implementation of weighted ENO schemes. *J. Comput. Phys.*, 126:202–228, 1996.

[20] K. Kailasanath, E. S. Oran, J. P. Boris, and T. R. Young. Determination of detonation cell size and the role of transverse waves in two-dimensional detonations. *Combust. Flame*, 61:199–209, 1985.

[21] A. Lafon and H. C. Yee. Dynamical approach study of spurious steady-state numerical solutions for non-linear differential equations, Part IV: Stability vs. numerical treatment of non-linear source terms. *Comp. Fluid Dyn.*, 6:89–123, 1996.

[22] A. Lafon and H. C. Yee. Dynamical approach study of spurious steady-state numerical solutions of nonlinear differential equations, Part III. the effects of nonlinear source terms in reaction-convection equations. *Comp. Fluid Dyn.*, 6:1–36, 1996.

[23] R. J. LeVeque and H. C. Yee. A study of numerical methods for hyperbolic conservation laws with stiff source terms. *J. Comput. Phys.*, 86:187–210, 1990.

[24] R.J. LeVeque and K.-M. Shyue. One-dimensional front tracking based on high resolution wave propagation methods. *SIAM J. Sci. Comput.*, 16:348–377, 1995.

[25] A. Majda and V. Roytburd. Numerical study of the mechanisms for initiation of reacting shock waves. *SIAM J. Sci. Stat. Comput.*, 11:950–974, 1990.

[26] F. Miniati and P. Colella. A modified higher order godunovs scheme for stiff source conservative hydrodynamics. *J. Comput. Phys.*, 224:519–538, 2007.

[27] D. Nguyen, F. Gibou, and R. Fedkiw. A fully conservative ghost fluid method & stiff detonation waves. *Proceedings of the 12th International Detonation Symposium, S. Diego, CA*, 2002.

[28] R. Pember. Numerical methods for hyperbolic conservation laws with stiff relaxation, I. spurious solutions. *SIAM J. Appl. Math.*, 53:1293–1330, 1993.

[29] C.-W. Shu and S. Osher. Efficient implementation of essentially non-oscillatory shock-capturing schemes. *J. Comput. Phys.*, 77:439–471, 1988.

[30] C.-W. Shu and S. Osher. Efficient implementation of essentially non-oscillatory shock capturing schemes, II. *J. Comput. Phys.*, 83:32–78, 1989.

[31] G. Strang. On the construction and comparison of difference schemes. *SIAM J. Numer. Anal.*, 5:506–517, 1968.

[32] V. Ton. Improved shock-capturing methods for multicomponent and reacting flows. *J. Comput. Phys.*, 128:237–253, 1996.

[33] L. Tosatto and L. Vigevano. Numerical solution of under-resolved detonations. *J. Comput. Phys.*, 227:2317–2343, 2008.

[34] Z. Xu and C.-W. Shu. Anti-diffusive flux corrections for high order finite difference WENO schemes. *J. Comput. Phys.*, 205:458–485, 2005.